Trace gas and radical diurnal behavior in the marine boundary layer during INDOEX 1999

J. Burkert,[1] M. D. Andrés-Hernández,[1] L. Reichert,[1] J. Meyer-Arnek,[1] B. Doddridge,[2] R. R. Dickerson,[2] J. Mühle,[3] A. Zahn,[3,4] T. Carsey,[5] and J. P. Burrows[1]

Received 24 July 2002; revised 21 November 2002; accepted 2 January 2003; published 17 April 2003.

[1] Selected trace gas mixing ratios (i.e., peroxy radicals ($RO_2^* = HO_2 + \Sigma RO_2$), nonmethane hydrocarbons (NMHCs), O_3, CO, HCHO, and NO) and photolysis rate coefficients of $j(NO_2)$ and $j(O(^1D))$ were measured in the marine boundary layer (MBL) over the Indian Ocean. The measurements were performed during February, March, and April 1999 as a part of the Indian Ocean Experiment (INDOEX) on board the research vessel R/V *Ronald H. Brown*. During the campaign, air parcels having different origins and consequently variable compositions were encountered, but all air masses, including those heavily polluted with NMHCs and aerosols, were in the regime of rapid photochemical ozone destruction. The influence of aerosols on the photolysis frequencies was investigated by comparison of measurements and results from the radiative transfer model PHOTOST: the high optical depth (up to 0.6) and low single scattering albedo of the aerosol reduces the UV flux at the surface substantially downwind of India and Arabia causing, for instance, a reduction in $j(O(^1D))$ by up to 40%. The diurnal behavior of the trace gases and parameters in the MBL has been investigated by using a time-dependent zero-dimensional chemical model. Significant differences between the diurnal behavior of RO_2^* derived from the model and observed in measurements were identified. The measured HCHO concentrations differed from the model results and are best explained by some missing chemistry involving low amounts of Cl. Other possible processes describing these two effects are presented and discussed. *INDEX TERMS:* 0322 Atmospheric Composition and Structure: Constituent sources and sinks; 0365 Atmospheric Composition and Structure: Troposphere—composition and chemistry; 3307 Meteorology and Atmospheric Dynamics: Boundary layer processes; 3339 Meteorology and Atmospheric Dynamics: Ocean/atmosphere interactions (0312, 4504); *KEYWORDS:* peroxy radicals, INDOEX, chlorine, nonmethane hydrocarbons, photolysis frequencies, formaldehyde

Citation: Burkert, J., M. D. Andrés-Hernández, L. Reichert, J. Meyer-Arnek, B. Doddridge, R. R. Dickerson, J. Mühle, A. Zahn, T. Carsey, and J. P. Burrows, Trace gas and radical diurnal behavior in the marine boundary layer during INDOEX 1999, *J. Geophys. Res.*, *108*(D8), 8000, doi:10.1029/2002JD002790, 2003.

1. Introduction

[2] The accurate measurement of trace gases over the ocean provides a particularly useful approach to assess the accuracy of atmospheric chemical models, because the simple dynamics and the lack of anthropogenic emissions, reduce the number of physicochemical processes required to describe and interpret the results. This study describes trace gas and free radical measurements made in the remote marine boundary layer (MBL), during INDOEX an international research initiative, proposed to study chemistry of remote regions of the Indian Ocean and the influence of outflow from the Indian subcontinent on these regions [see *Crutzen and Ramanathan*, 2001; *Ramanathan et al.*, 2001; *Lelieveld et al.*, 2001; *Ball et al.*, 2003] (see also http://www-indoex.ucsd.edu).

[3] The chemistry of the remote and pristine MBL is currently considered to be initiated by the photolysis of O_3. The subsequent reaction of $O(^1D)$ with H_2O is both the dominant loss of O_3 and yields the most important daytime tropospheric oxidizing agent, the OH radical [*Levy*, 1971]:

$$O_3 + h\nu(\lambda < 320\ \text{nm}) \rightarrow O(^3P) + O_2 \quad (1)$$

$$O(^1D) + O_2 \quad (2)$$

[4] Peroxy radicals ($RO_2^* = HO_2 + \Sigma RO_2$; being R = organic group) formed in the oxidation of CO, CH_4 and

[1]Institute of Environmental Physics, University of Bremen, Bremen, Germany.
[2]Department of Meteorology, University of Maryland, College Park, Maryland, USA.
[3]Air Chemistry Division, Max Planck Institute for Chemistry, Mainz, Germany.
[4]Now at Institute of Meteorology and Climate Research, Forschungszentrum Karlsruhe, University of Karlsruhe, Karlsruhe, Germany.
[5]Atlantic Oceanographic and Meteorological Laboratories, National Oceanic and Atmospheric Administration, Miami, Florida, USA.

0148-0227/03/2002JD002790$09.00

NMHC (nonmethane hydrocarbons) play a significant role in the production and depletion cycles of ozone (O_3).

$$OH + CO + M \rightarrow HOCO + M \quad (3)$$

$$HOCO + O_2 \rightarrow HO_2 + CO_2 \quad (4)$$

$$OH + CH_4 \rightarrow CH_3 + H_2O \quad (5)$$

$$CH_3 + O_2 + M \rightarrow CH_3O_2 + M \quad (6)$$

[5] The reaction of NO with RO_2^* and the subsequent NO_2 photolysis produces O_3 in a catalytic cycle, which is now well established [*Lightfoot et al.*, 1992; *Burkert et al.*, 2001a, and references therein].

[6] In addition to the O_3 removal via reactions (1) and (2) another important loss is initiated by the reaction of O_3 with HO_2 (reaction (7)) leading to a cycle together with the reactions (3) and (4).

$$HO_2 + O_3 \rightarrow OH + 2O_2. \quad (7)$$

[7] The competition between the production and loss of O_3 determines the amount of O_3 and its temporal behavior at a given location. The compensation point, i.e., the amount of NO_x ($NO_x = NO + NO_2$) in a given air parcel, where the rate of production of O_3 is equal to the rate of loss of O_3 depends on the assumed conditions [*Crutzen*, 1973; *Lightfoot et al.*, 1992]. Typical NO_x mixing ratios for the compensation point in remote areas vary between ~10–40 pptv, depending primarily on the O_3 concentration present.

[8] For low-NO_x, the RO_2^* self reactions gain importance compared to the reaction of RO_2^* with NO. The RO_2^* are key intermediates in the photochemical processes generating peroxides (e.g., CH_3OOH, and H_2O_2) and in the subsequent production of HCHO.

$$HO_2 + HO_2 \rightarrow H_2O_2 + O_2, \quad (8)$$

$$CH_3O_2 + HO_2 \rightarrow CH_3OOH + O_2 \quad (9)$$

$$CH_3OOH + h\nu \rightarrow CH_3O + OH \quad (10)$$

$$CH_3O + O_2 \rightarrow HCHO + HO_2 \quad (11)$$

[9] One result of the pre-INDOEX studies was the clear observation of strong diurnal cycling of O_3 having a minimum during the day, [*Rhoads et al.*, 1997]. Similar but generally weaker cycling has been occasionally observed in the most remote regions of the Atlantic Ocean from the German research vessels the Polarstern and Meteor in a series of cruises from 1987 to 1996 [*Burkert et al.*, 2001b]. In addition to the loss of O_3 by the reaction with HO_2 (reaction (7)), evidence for a significant role of reactive halogens in the chemistry of the pristine MBL was inferred from an analysis of the pre-INDOEX observations [*Dickerson et al.*, 1999].

[10] This study describes the measurements of RO_2^*, NO, NMHC, $j(NO_2)$, $j(O(^1D))$ and O_3 made from the National Oceanic and Atmospheric Administration (NOAA) research vessel R/V *Ronald H. Brown* in the MBL. These observations continued those made within AEROSOL campaign, which made measurements from Norfolk Virginia via the North and South Atlantic into the Indian Ocean [*Andrés-Hernández et al.*, 2001].

[11] The cruise track of the R/V *Ronald H. Brown* during INDOEX was similar to the track of the pre-INDOEX cruise, which took place during the fall of 1995 [*Rhoads et al.*, 1997]. One overarching goal of the AEROSOL and INDOEX campaign is to improve our knowledge of the fast photochemistry of the MBL. Specific objectives of this study are to assess the impact of aerosols on photolysis rates, the role of continental emissions on pollution levels in the remote marine atmosphere, and the link between levels of O_3 and RO_2^*. To achieve this objective the measured concentrations and diurnal variation of RO_2^* and HCHO [*Wagner et al.*, 2001], predicted by a zero-dimensional chemical model of the MBL have been compared with those measured to assess the possible role of multiphase and halogen chemistry in the budget of this species. The different behavior of the observed amounts of RO_2^* above the Atlantic and the Indian Ocean is also discussed in this study.

[12] The following scientific issues and questions are raised and discussed in this paper: How do aerosols influence the photolysis frequency at ground level? Are the current parameterizations for the radiative properties suitable and appropriate? Are the measured amounts of RO_2^* in agreement with that predicted by box model simulations? Are the observations of RO_2^* and HCHO consistent and do they reflect the close chemical linkage between these constituents? Is the difference between HCHO measurements and model results observed during INDOEX different to the observations above the Atlantic Ocean [*Weller et al.*, 2000]? Does the presence of 1×10^4–1×10^5 molecules cm^{-3} amounts of reactive halogens provide a reasonable and plausible explanation of the unexpected behavior of RO_2^* and HCHO? What are the potential sources of reactive chlorine and bromine in the remote MBL? Do geographical or regional effects help to explain the difference between model results and measurements?

2. Experimental Techniques

2.1. RO_2^*, and CO Measurements

[13] Peroxy radicals were measured continuously during the INDOEX campaign by using the chemical amplification technique (PERCA). This measurement technique is based on the conversion of peroxy and oxy radicals into an amplified, NO_2-modulated signal. The latter is detected by the chemiluminiscence produced from the reaction of NO_2 with a Luminol solution [*Hastie et al.*, 1991; *Clemitshaw et al.*, 1997; *Burkert et al.*, 2001a]. The PERCA measures the sum of HO_2, OH, RO and RO_2 radicals, which to a good approximation can be considered to be equivalent to RO_2^*. The amplification of the signal, i.e., the

chain length (CL) of the chain reactions, and the conversion factor for the individual organic radicals must be determined by adequate calibrations. The radical calibration source utilize the photolysis of H_2O in air at 185 nm [*Schultz et al.*, 1995]. The PERCA and the calibration technique have been described in more detail elsewhere [*Hastie et al.*, 1991; *Volz-Thomas et al.*, 1998; *Burkert et al.*, 2001b].

[14] The RO_2^* data account for the water dependence of the CL first reported by *Mihele and Hastie* [1998], but characterized experimentally and interpreted for the sampling and detector chamber conditions used [*Reichert*, 2000; *Burkert et al.*, 2001b; *Reichert et al.*, 2003]. To date, there is no unambiguous explanation of this dependency, but the reactions of H_2O clusters and peroxy radical adducts ($HO_2.nH_2O$) appear best to explain the observed water vapor dependence of the CL [*Reichert et al.*, 2003].

[15] During INDOEX, NO_2 and radical calibrations for the PERCA were performed twice a day and once a week respectively. The average CL, determined from all the radical calibrations performed in dry air during the measurement period, was 159 for the first leg, 136 ± 13 for the second leg and 122 ± 13 for the third leg. The steady decrease of the CL, observed during the whole campaign, is most probably caused by increasing contamination of the 20 m long inlet system with sea salt, in spite of the regular cleaning of the reactor.

[16] The temperature and the relative humidity of air entering the PERCA were assumed to be that provided by the data system of the ship. The detection limit is estimated to be 3–5 pptv RO_2^* for 1-min values. The precision of peroxy radical calibrations is ~15% and a maximum uncertainty of ±30% is estimated for 1σ and 1 minute RO_2^* values.

[17] The inlet of the system was mounted on a mast located at the bow of the ship approximately 20 m above the sea level. The PERCA detector was inside an air-conditioned container on the deck. Trace gases O_3 and carbon monoxide were measured with a commercial UV photometer (TEI Model 49C, Franklin, MA) and modified commercial nondispersive infrared gas filter correlation analyzer (TEI model 48C, Franklin, MA), respectively [*Dickerson and Delany*, 1988; *Parsons and Dickerson*, 1999], acquired at 1-min resolution. The complete data set is reported by *Stehr et al.* [2002].

2.2. NO Measurements

[18] Nitrogen oxide was measured by a chemiluminescence detector built according to established protocols [e.g., *Carroll et al.*, 1985]. The instrument is described in previous publications [*Rhoads et al.*, 1997; *Carsey et al.*, 1997]. The detector was housed together with the PERCA, both inlets were fixed on the sampling tower. To avoid contamination by sea salt aerosols, the inlet line was capped by a 37-mm diameter 1-μm pore size Teflon filter (Gelman), replaced frequently during the cruise.

[19] Airflow through the system was set to 1.2 L min^{-1}. The flow rate was calibrated periodically throughout the cruise with a bubble-flowmeter (Sensidyne, Clearwater, Florida). A needle valve in the air line at the instrument rack further reduced the pressure and decreased gas travel time from the sampling point to the detector to less than 5 s. The NO was detected by measuring the chemiluminescent emission resulting from the reaction of NO with O_3 within a gold-coated stainless steel reaction chamber. Blank count rates were determined by reacting the gas stream with excess O_3 prior to entering the reaction chamber. The emitted photons were recorded by a 9658R photomultiplier tube (Thorn EMI) held at a potential of 1250 volts and contained in a cooled housing (Products For Research) maintained nominally at −40°C. Photon counting intervals of 10 s were recorded for the duration of the cycle. The first 2–3 minutes of each measure and calibrate count segments were ignored to allow the system to equilibrate. Each run was scanned for spikes or other anomalies due to other shipboard instrumentation. For the calibration a commercial calibration gas mixture (4.94 ppbv NO in N_2, Scott Specialty Gas) was injected into the inlet stream. Background count rates were higher than in previous experiments. The mixing ratios of NO were obtained by subtracting the daytime (10 a. m. to 2 p. m. local time) average mixing ratios, from that obtained at night (10 p. m. to 2 a. m. local time).

2.3. j(NO_2) Measurements

[20] The frequency of photodissociation of NO_2 to NO and $O(^3P)$ was measured by determining the production of NO in a flow of NO_2 through a glass reactor of length 20 cm and volume 10 cm^3 [*Kelley et al.*, 1995]. In the standard manner, a black surface beneath the detector, yields the photolysis frequency of NO_2, j(NO_2):

$$j(NO_2) = \int I(2\pi).\phi(NO_2, \lambda)\sigma(NO_2, \lambda)d\lambda$$

[21] Where $I(2\pi)$ is the downwelling light flux at the surface, $\phi(NO_2, \lambda)$ the quantum yield for the dissociation of NO_2 and $\sigma(NO_2, \lambda)$ the absorption cross section of NO_2.

[22] 2l min^{-1} of a mixture of NO_2 and air flowed constantly through the system. The NO and NO_2 mixing ratios were determined using a commercial detector (TEI model 42, Franklin, MA). The uncertainty with 95% confidence is estimated to be ±7% for values above 3×10^{-3} s^{-1} for 1 min average.

2.4. j($O(^1D)$) Measurements

[23] The actinic UV flux was measured using a 2πsr filter radiometer with isotropic sensitivity (Meteorologie Consult GmbH, Germany), described by *Junkermann et al.* [1989] but having a filter combination optimized for cloudy conditions and high solar zenith angles. The O_3 column necessary to convert the recorded actinic UV flux into an O_3 photolysis frequency, j($O(^1D)$), was measured many times each day aboard the R/V *Ronald H. Brown* using a hand-held Microtops II sunphotometer (S/N 3685), having a 1–2% precision [*Meywerk and Ramanathan*, 2002]. The filter radiometer was compared with a spectroradiometer, described by *Hofzumahaus et al.* [1999], immediately after the INDOEX campaign. The j($O(^1D)$) values ranged between 0 and $2.2 \times 10^{-5} s^{-1}$. The regression line exhibited a slope of 1.0; the linear correlation coefficient r^2 being 0.9989. The total uncertainty of the j($O(^1D)$) data presented here is 15–20% for solar zenith angles (SZA) below 60°, increasing to 50% at SZA = 80° (including the current

uncertainties in the O_3 absorption cross section and $O(^1D)$ quantum yield).

2.5. NMHC Measurements

[24] Altogether 59 air samples, each having a volume of 9 L (STP), were collected in 2.5 L electropolished stainless steel canisters for the laboratory based analysis of NMHC. The air was sucked from the top of the bow tower (10 m height) via a stainless steel tube. Except during transport (~6 days) to the analytical laboratory (MPI–C, Mainz, Germany) the canisters were kept at −18°C and then equilibrated at ambient temperature for 12 h before gas chromatographic analysis. The condensable compounds (encompassing the NMHC) were first cryogenically concentrated at −170°C in a microtrap packed with porous silica beads, and thereafter, were separated on a Al_2O_3/KCl porous layer open tubular (PLOT) column connected to a quadrupole mass spectrometer (HP 5973). Laboratory tests indicated detection limits (3σ variation of a blank sample) of 0.2–6.8 pptv for ethane, propane, butane, isobutane, pentane and isopentane, and 14–26 pptv for acetylene. The precision for all species is 5–10%. Comparisons with other laboratories showed agreements within ~20%, for all species addressed here. For details, see *Mühle et al.* [2002].

2.6. Other Supporting Measurements

[25] The meteorological parameters and back-trajectory analysis were taken from the INDOEX database and from the NOAA Pacific Marine Environmental Laboratory (PMEL) (for further information see http://www-indoex.ucsd.edu/index.html and http://saga.pmel.noaa.gov/indoex/index.html).

2.7. Modeling

[26] The model, developed to simulate and investigate the chemical mechanism of the remote MBL, solves the time-dependent set of differential equations using the atmospheric chemistry package ASAD (A Self-contained Atmospheric chemistry coDe) [*Carver et al.*, 1997]. The chemical scheme accounts for 95 species and describes the chemistry of CH_4, CO, dimethylsulfide (DMS) and selected NMHC (C_2H_2, C_2H_4, C_2H_6, C_3H_6, C_3H_8) [*Burkert et al.*, 2001b]. The oxidation of NMHC and DMS was assumed to produce HCHO or peroxy radicals in their reaction pathways, if the products of their reaction are unknown. The chemistry of the MBL is described by 149 bimolecular, 30 termolecular and 21 photolysis reactions. Additionally the physical deposition of H_2O_2, CH_3OOH and O_3 at the sea surface is appropriately modeled. The reactions and reaction rate coefficients have been collated from the IUPAC [*Atkinson et al.*, 2000], JPL [*DeMore et al.*, 1997] and NIST (National Institute of Standards and Technology) Chemical Kinetics Databases. The model does not take into account the dynamics, for example mixing, advection or convection, and the remote marine boundary layer is considered to be an effectively well mixed chemical reactor.

3. Result

3.1. Definition of Air Masses, Encountered During INDOEX

[27] Making use of the 6 days back-trajectories and the measurements of chemical and aerosol composition, four different types of dynamical regimes could be defined during the campaign [*Ball et al.*, 2003]:

[28] 1. Southern Hemisphere maritime Equatorial (SHmE), characterized as having a long transport over relatively pristine regions.

[29] 2. Northern Hemisphere maritime Equatorial (NHmE), characterized as having passed over relatively unpolluted regions.

[30] 3. Northern Hemisphere continental Tropical (NHcT), the air floss-passing over India.

[31] 4. Northern Hemisphere continental extratropical (NHcX), the air flows passing over the Arabian Peninsula.

[32] The cruise tracks and the daily position are presented in Figure 1. The prevailing airflow patterns during the three legs of INDOEX are shown in Figure 2. These overall patterns of air movement represent the average situation but there is significant local, spatial, and temporal variability.

3.2. Characteristics of the Different Air Masses Observed During the 3 Legs of INDOEX

[33] The four different air masses exhibited the following characteristics.

3.2.1. SHmE Observed During DOY 54–58, 78.25–79.5

[34] The SHmE regime showed the lowest mixing ratios for all trace species and in this sense was the least polluted air encountered. The maximum RO^*_2 mixing ratio during DOY 54–58, decreased with decreasing latitude from 35 to 25 pptv. The O_3 mixing ratio revealed the same behavior, decreasing from 15 to 8 ppbv. The loss of O_3 per latitude decreases with decreasing latitude. The mean CO mixing ratio was 56 ppbv, the daytime average NO mixing ratio was below the detection limit of around 3 pptv. The NMHC mixing ratios were the lowest observed during the whole campaign. The mean values were: ethane 194 pptv, propane 7 pptv, and acetylene 21 pptv [*Mühle et al.*, 2002]. The vertical profiles of O_3 mixing ratio showed a weak positive gradient with increasing altitude up to 12 km between 12°S and the ITCZ, where the O_3 reached levels about 40 ppbv (H. Smit, personal communication 2001).

3.2.2. NHmE Observed During DOY 76–78.25, 79.5–81

[35] In the NHmE regime the CO and O_3 mixing ratios were around 90 ppbv and approximately 10 ppbv, respectively. The maximum RO^*_2 mixing ratio varied between 55–60 pptv. The back-trajectories indicate a long travel time of the air parcel along the west coast of India. The NO mixing ratio was below the detection limit. Most of the NMHC doubled their mean mixing ratios compared to the SHmE air mass: ethane 332 pptv, propane 10 pptv, and acetylene 44 pptv. The vertical profiles of O_3 in this regime indicate an even weaker positive gradient in altitude compared to the SHmE regime, reaching levels of about 30 ppbv at 12 km.

3.2.3. NHcT Observed During DOY 63–66, 74–76, 85–89

[36] The NHcT regime was characterized by the highest observed maximum mixing ratios in RO^*_2 and CO during the whole campaign. Maximum levels of up to 90 pptv RO^*_2 and 200 ppbv CO were observed. NO measurements were higher than in the SHmE, but still close to the detection

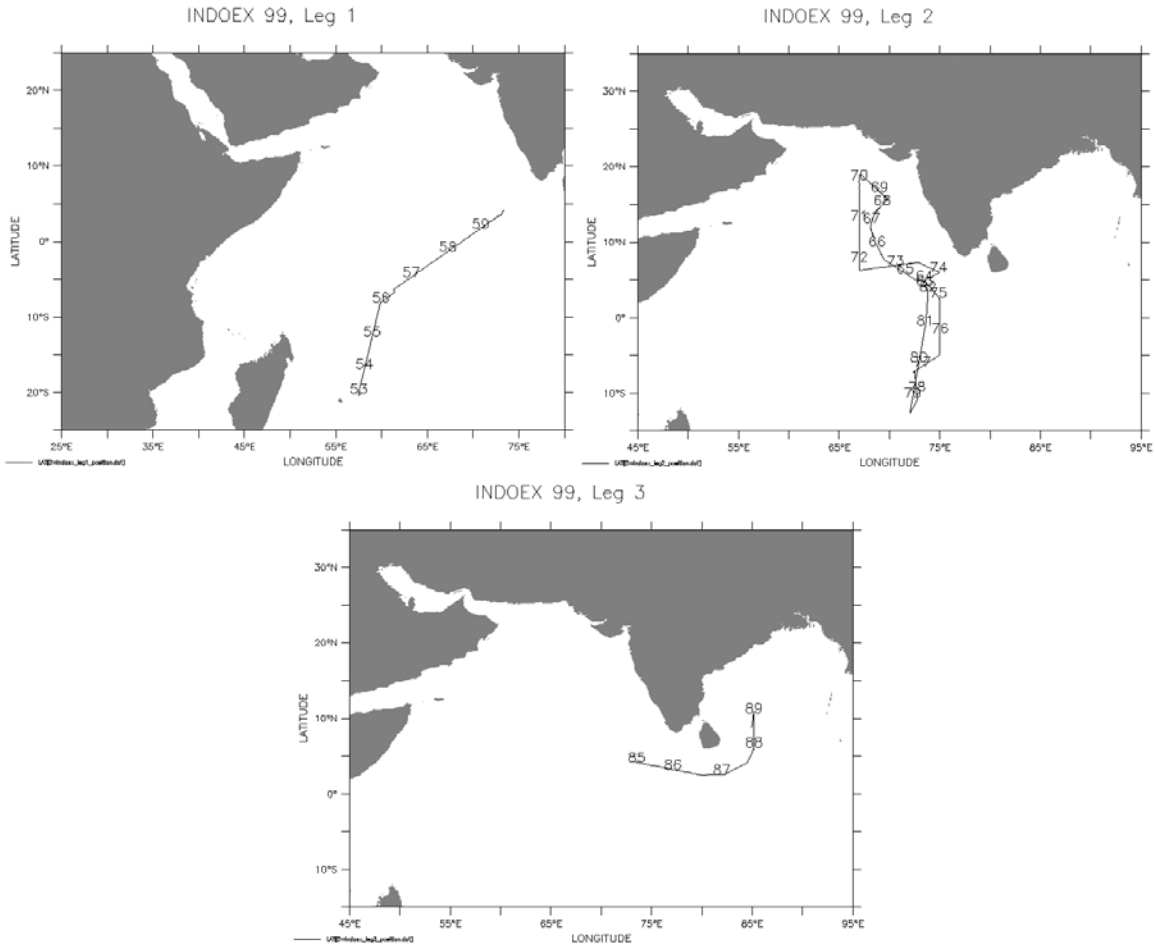

Figure 1. INDOEX cruise tracks for leg 1–3, numbers along the track indicate day of the year (DOY).

limit, around 6 pptv. The O_3 mixing ratios showed strong diurnal variations, with O_3 losses during the day being as large as 50%. The latitudinal gradient in O_3 was ~1.25 ppbv/°latitude heading north. The NMHC main mixing ratios increase for ethane up to 403 pptv, propane to 20 pptv, and acetylene to 133 pptv. The vertical O_3 profiles revealed an enriched layer between 1 and 3 km having mixing ratios larger than 70 ppbv. The upper level O_3 values were different depending on the periods of observation. Back-trajectory analysis indicates that the air masses originated over India and the Bay of Bengal. The NHcT regime also appears to contain high concentrations of ash, soot, and other organic matter [*Dickerson et al.*, 2002; *Neusuess et al.*, 2002; *Quinn et al.*, 2002]. In addition the regime is heavily contaminated by fossil fuel combustion (indicated by sulphate), biomass burning (indicated by nss-potassium), and wind-blown mineral dust (indicated by ash and nss-calcium) [*Ball et al.*, 2003; *Quinn et al.*, 2002; *Stehr et al.*, 2002]. The black carbon from India is currently considered to result mainly from internal combustion engines, biomass burning, and small-scale coal combustion. However, bottom-up estimates of black carbon emissions from India yield much smaller values than do in situ observations. This suggests an additional source not considered yet or unusually high emissions factors [*Dickerson et al.*, 2002]. Therefore a large uncertainty in the sources and/or emissions remains.

3.2.4. NHcX Observed During DOY 66–74

[37] The NHcX regime was characterized by the highest observed concentration of O_3 and NMHC at the most northerly point of the whole campaign. O_3 mixing ratios reached levels up to 53 ppbv and the NMHC averaged mixing ratios were: ethane 927 pptv, propane 133 pptv, and acetylene 169.3 pptv. The latitudinal gradient in O_3 remained ~1.25 ppbv/°latitude heading north. RO_2^* and CO varied weakly around 55 pptv and 122 ppbv respectively. NO mixing ratios reached their highest values of the campaign being approximately 9 pptv. The vertical profile in O_3 showed the same behavior as in the NHcT regime with an O_3 enriched layer above the MBL. The back-trajectories indicate that the air masses originated over the Arabian Peninsula.

3.3. Measurements Trace Constituents and Parameters Aboard the R/V *Ronald H. Brown*

3.3.1. Radical and Trace Gases: RO_2^*, O_3, and CO Measurements for Legs 1, 2, and 3 of INDOEX

[38] RO_2^*, O_3, and CO were continuously measured from DOY 54 to DOY 89. The observed RO_2^*, O_3, and CO diurnal cycles for the three legs are presented in Figure 3. The RO_2^* mixing ratios showed the typical diurnal variation with the maximum occurring between midday and early afternoon. The RO_2^* daytime maximum values vary from

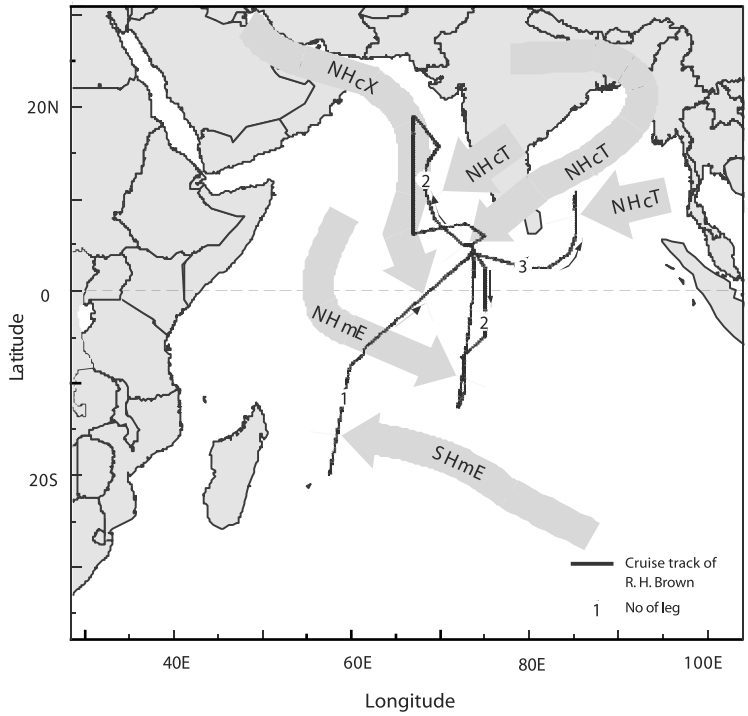

Figure 2. Cruise track of the R/V *Ronald H. Brown* during the 1999 INDOEX campaign and the cluster trajectories (950 hPa) showing the origin of the air masses encountered during the different segments of the cruise. The flow regimes are labeled SHmE, Southern Hemisphere marine equatorial; NHmE, Northern Hemisphere marine equatorial; NHcT, Northern Hemisphere continental tropical (subdivided in the subregimes Bengal and west); and NHcX, Northern Hemisphere continental extratropical.

25 to 90 pptv. CO concentrations did not show any significant diurnal variation, they only changed with different air masses. The CO values varied in the NH between 100 and 200 ppbv and in the SH between 40 and 70 ppbv.

[39] The O_3 mixing ratio, typically, decreases during daytime with a minimum close to sunset and a recovery during the night. In contrast to this behavior the O_3 in leg 1 does not show any recovery at night and each day the average O_3 mixing ratio is smaller. This implies that the net photochemical losses during the day are equal to the latitudinal variation of O_3. The maximum values of O_3 varied in the SH between 8 and 15 ppbv and in the NH between 10 and 55 ppbv.

3.3.2. NO Data

[40] The NO data collection for INDOEX began on DOY 53. The average mixing ratio of NO in the SHmE air mass was 3 pptv, being comparable to the 4.8 pptv reported for the SHmE regime [*Rhoads et al.*, 1997]. The average mixing ratio for NO within NHcT was 6 pptv, compared to 4.7 pptv found in the earlier cruise.

[41] A summary of the measurements of NO associated with the different air mass type is given in Table 1. The largest mixing ratios of NO were found within the NHcX air mass, where input from the Indian continental regions is expected to be low and the travel time over the ocean relatively long compared with that for the other air mass types, being about 3–5 days. Therefore the NO was most likely transported in the upper layers of the troposphere, where the lifetime of NO is much longer compared to the MBL.

3.3.3. j($O(^1D)$) and j(NO_2) Photolysis Frequency Measurements

[42] In Figure 4, the measured j($O(^1D)$) and j(NO_2) photolysis frequencies for, leg 2 of INDOEX and two selected days in the NH and SH, respectively, are shown. The variation in the maximum j($O(^1D)$) values indicates the large influence of the aerosols on the photolysis frequencies. The reduction is about 40% for j($O(^1D)$) and about 22% for j(NO_2).

[43] Taking into account that more than half of the light driving the photolysis of O_3 to $O(^1D)$ is scattered "skylight" rather than direct sunlight, the sometimes observed small cumulus clouds have little impact and the assumption of clear sky conditions for the model used later on is therefore reasonable.

3.3.4. NMHC Measurements

[44] The NMHC measurements have been separated into the amounts of smaller (C < 5) and larger (C > 4) alkanes and are presented in Figure 5. Some of the data have already been presented by *Mühle et al.* [2002]. The highest amount of all alkane was observed in the NHcX regime, moderate levels being present in the NHcT regime and the lowest values were encountered in the NHmE: the latter being around half of that in the NHcT regime. The transition between NHcT and NHmE was gradual, and not as sharp as the transition between other air masses. Air masses, influenced by the Arabian Peninsula, contain the highest amounts of NMHC: the daily peak being up to twice as high as the average concentration.

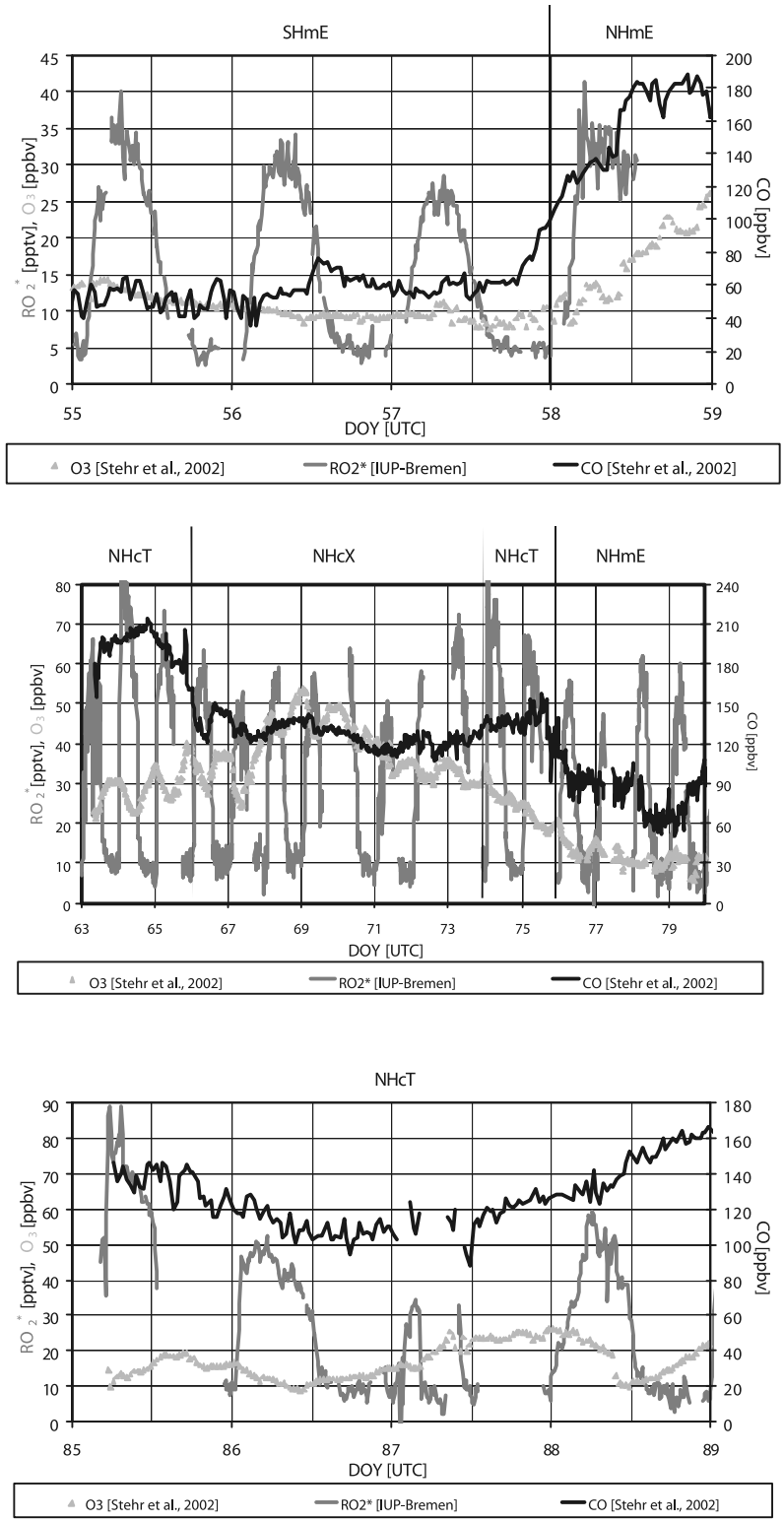

Figure 3. Plots of the individual diurnal variation of RO_2^*, O_3, and CO observed on legs 1 to 3 of INDOEX. The classification of the air masses encountered are written above the days and vertical lines separate the different types of air masses.

Table 1. Averaged NO Mixing Ratios Observed in Four Different Air Masses[a]

Air Mass Design	NO mixing ratio Mean, pptv	Standard Deviation	Number of Measurements, 24 Hour Average
SHmE	3	5	6
NHcT	6	11	7
NHcX	9	8	6
NHmE	below detection limit	–	2

[a]Mixing ratios were computed as day-night differences.

[45] The observed decrease in the measured concentrations of the NMHC on DOY 66, 67, 72, and 73 cannot be explained by chemical destruction but rather by transport effects. The 800 mbar back trajectories, which originated over India, indicate an increasing downward mixing of NHcT air masses into the NHcX air masses in the MBL.

4. Discussion and Interpretation

[46] In this section the measurements of trace constituents and parameters are analyzed. Initially the photolysis frequencies, which were determined by calculation in the model, are compared with the ground based measurements. The role of aerosol on the photolytic radiation in the MBL is then discussed. Accurate knowledge of the photolysis frequencies is required as input for the chemistry of the box model.

4.1. Simulation of Photolysis Frequencies in the MBL During INDOEX and the Influence of Aerosol Scattering

[47] Photolysis frequencies for the photolytic active trace gases were calculated in this study using PHOTOST, an improved version of the model PHOTOGT [*Blindauer et al.*, 1996], which has been upgraded to use the radiative transfer model (RTM) SCIATRAN [*Buchwitz*, 2000] in place of its predecessor GOMETRAN [*Rozanov et al.*,

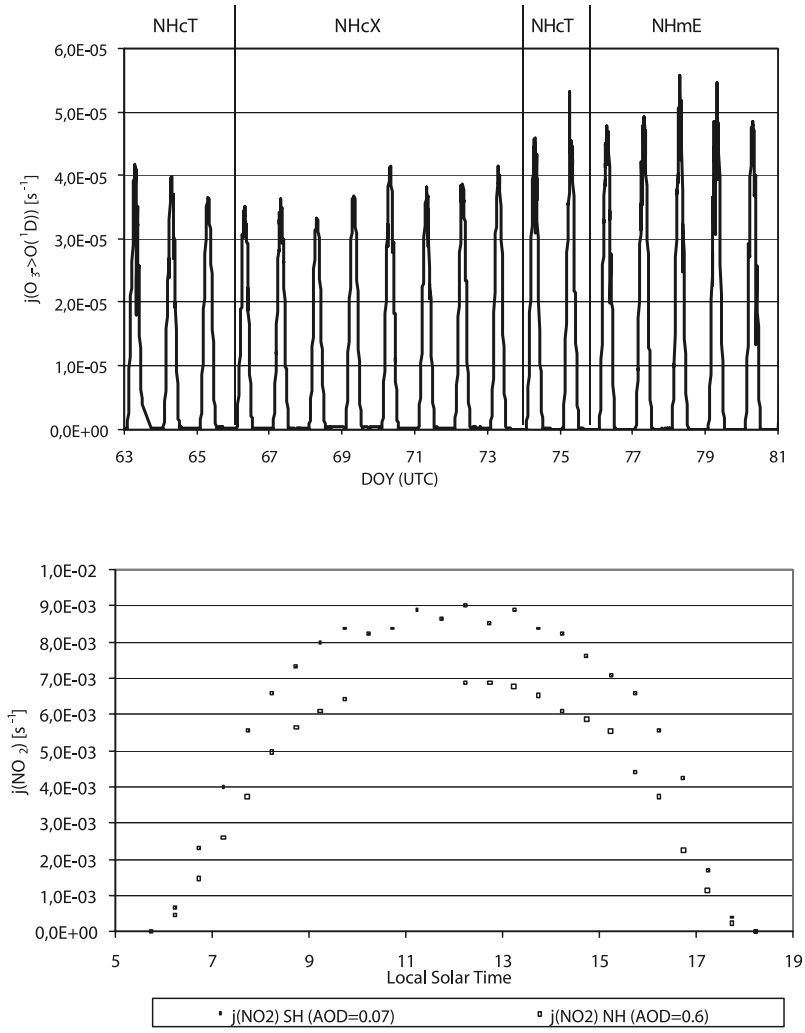

Figure 4. (a) Measured j($O(^1D)$) photolysis rates for leg 2 (DOY 63–80) during INDOEX. (b) Diurnal variation in the photolysis rate coefficient for NO_2; only cloud-free data are shown. Filled squares represent data from the clean, marine atmosphere on DOY 57 at 4°S with an AOD of about 0.07 at 500 nm. Open squares represent data from a polluted atmosphere over the northern Indian Ocean on DOY 65 at 6°N with an AOD of 0.4 at 500 nm.

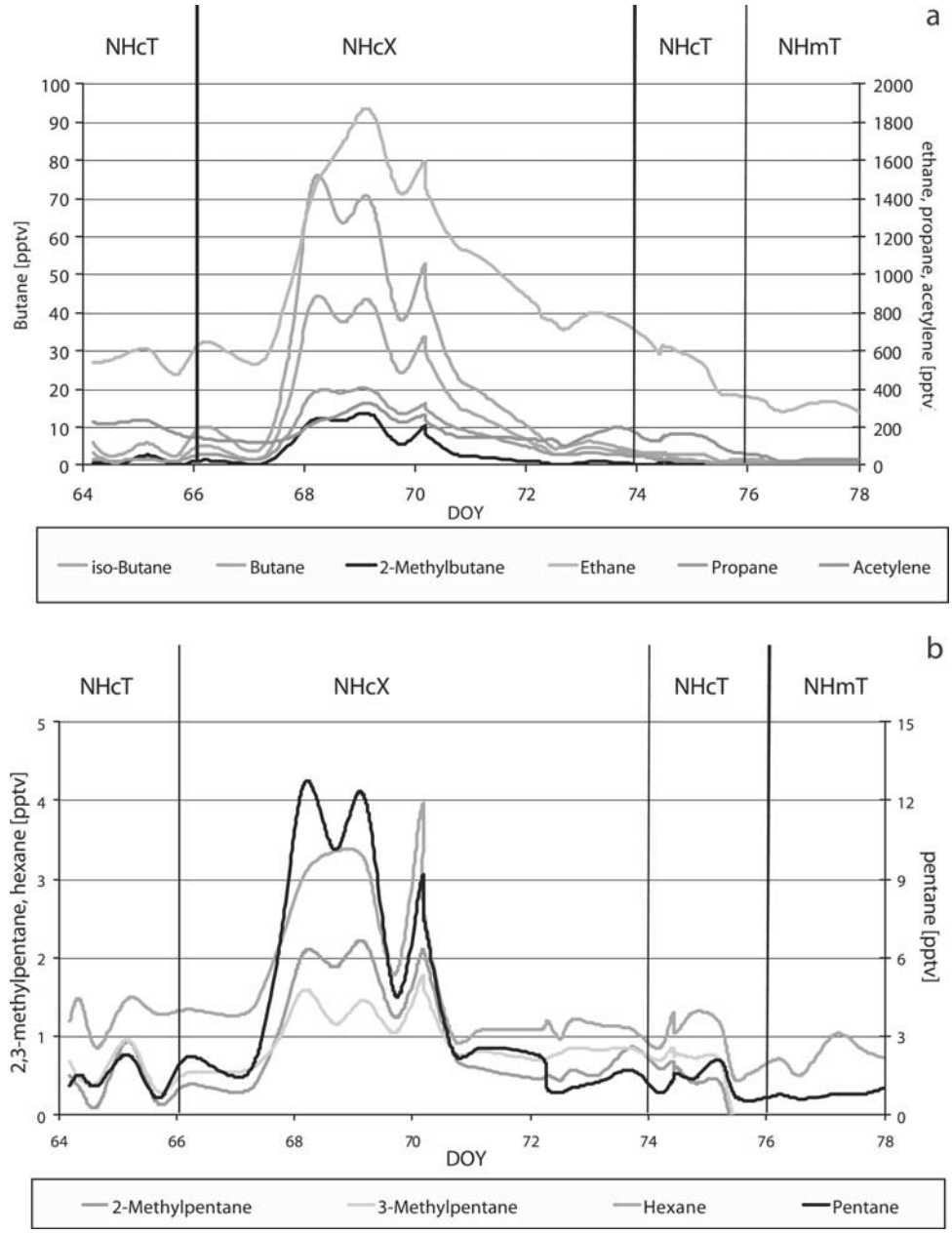

Figure 5. NMHC alkane measurements in the NH during INDOEX (DOY 64–78) (a) the lighter alkanes and (b) the heavier alkanes measured. See color version of this figure at back of this issue.

1998]. To initialize the RTM, the in situ measurements of the aerosol optical depth (AOD) made during INDOEX were used [*Welton et al.*, 2002]. These agreed with the observed Sun photometer measurements [*Meywerk and Ramanathan*, 1999; *Welton et al.*, 2002]. The photolytic radiation, encountered in the MBL during the INDOEX campaign, was determined in the model taking explicitly into account the following:

[48] 1. Rayleigh single and multiple scattering by air molecules,

[49] 2. O_3 absorption of ultraviolet radiation, the values of total O_3 column being those measured by GOME on board the ERS-2 satellite [*Burrows et al.*, 1999, and references therein], all other trace gases were taken from a climatology database [*Bruehl and Crutzen*, 1993].

[50] 3. The effective surface spectral reflection at the ocean surface, albedo (α = 0.05). The underestimation of the actinic flux on account of neglecting the SZA dependence of the albedo is below 1% (SZA = 60°), 2.5% (SZA = 70°), 6% (SZA = 80°), and 8% (SZA = 90°) [*Cox and Munk*, 1954; *Jin et al.*, 2002].

[51] 4. Single and multiple scattering and absorption by aerosol, the aerosol parameters being defined in the model such that the aerosol composition and the aerosol optical depth (AOD) were compatible with the in situ and Sun photometer measurements.

[52] During INDOEX the aerosol composition of the MBL was continuously measured at the island station of Kaashidoo [*Lelieveld et al.*, 2001]. The average of the entire data set is shown in Table 2a and is used to describe the

Table 2a. Averaged Aerosol Composition Measured at Kaashidoo During the INDOEX Campaign[a]

Type	Dry Mass, %
Sulfate	31
Organics	25
Black carbon	15
Mineral dust	11
Ammonia	9
Fly ash	6
Minor components	3

[a]From *Lelieveld et al.* [2001].

aerosol composition in the model. The atmosphere above the MBL contains only the Kaashidoo compositions, whereas the MBL contains a mixture between the (1) Kaashidoo aerosol composition (Table 2a) and (2) sea salt aerosol composition (Table 2b), as described in Table 2c.

[53] The average daily measurements of the AOD [*Welton et al.*, 2002] were used. The diurnal variation in aerosol composition was not taken into account. Analysis using the LOWTRAN-7 parameterization for several different types of aerosols indicates that changes in the aerosol composition within the range of that observed in INDOEX, have only a negligible effect on the photolytic radiation field in the MBL. This assumption is supported by comparing the measured single scattering albedo of 0.874 ± 0.028 at 500 nm for the INDOEX period at Kaashidoo island [*Bush and Valero*, 2002] and our calculated value of 0.882 for this region. For the whole campaign the single scattering albedo values varied between 0.882 for the most polluted case and 0.932 for the SH region encountered during the campaign.

[54] The profile of the aerosol extinction, $\alpha(\lambda, z)$ [km^{-1}] was obtained by using the LOWTRAN-7 aerosol profiles [*Shettle and Fenn*, 1976] for different scenarios, but modifying them in the lowest 5 km of the troposphere in order to fit the measured AOD (Figure 6).

$$\mathrm{AOD}(\lambda) = \int_{z_1}^{z_2} \alpha(\lambda, z)\mathrm{d}z. \qquad (12)$$

[55] In situ measurements of the aerosol extinction coefficient with respect to height have been performed on board the R/V *Ronald H. Brown* [*Welton et al.*, 2002]. The measured photolysis frequencies shown in Figures 7, 8, 9, and 10 are based on 2πsr, whereas the model results are for 4πsr. Therefore all measured photolysis frequencies for 4πsr should be approximately 5–7% higher to account for the upwelling flux caused by the reflection at the ocean surface.

[56] Figure 7 shows the modeled photolysis frequencies $j(O(^1D))$ and $j(NO_2)$ for AOD varying between 0.0 and 0.6, versus sec(SZA). The results show, that the influence of the aerosols varies with the SZA. The $j(O(^1D))$ rate for AOD = 0.0 decreases up to 23% for AOD = 0.6 for sec(SZA) = 1,

Table 2b. Typical Sea Salt Aerosol Composition[a]

Type	Dry Mass, %
Water soluble	7.1
Sea salt (accumulation mode)	90.8
Sea salt (coarse mode)	2.1

[a]From *Shettle and Fenn* [1976].

Table 2c. MBL Mixing Between Tables 2a and 2b Assumed in the Model

DOY	Composition
55–57; 78	87% ss; 13% nss
58–60; 63–67; 85–88	18% ss; 82% nss
68–70	40% ss; 60% nss
71–76	33% ss; 67% nss
77; 79–82	65% ss; 35% nss

the relative effect decreases up to 39% for sec(SZA) = 2. The same behavior is observed for $j(NO_2)$, for sec(SZA) = 1 the relative decrease is 17% and for sec(SZA) = 2 the relative decrease is 37%.

[57] The calculated j values depend upon Rayleigh scattering (α_{ray}), trace gas absorption (α_{trace}), and Mie scattering (α_{Mie}, i.e., aerosol scattering). The influences of these three effects are wavelength-dependent. In general the α_{ray} and α_{trace} (e.g., O_3 and NO_2) are more important in the short wavelength region and α_{Mie} becomes more significant in the longer wavelength region. Therefore the relative influence of aerosols on the photolysis frequencies, as measured by the ratio j(AOD = 0.0)/j(AOD = 0.6), which varies with sec(SZA), is higher at longer wavelengths. Thus $j(NO_2)$, which is weighted toward 400 nm is expected to be more influenced by the presence of significant amounts of aerosol than $j(O(^1D)$, which is weighted toward 300 nm.

[58] In Figure 10, the correlation of simulated and measured $j(O(^1D))$ is plotted separated into different AOD regimes. Overall the agreement is reasonable, but in general the calculated j values underestimate the measured photolysis frequencies when lower AODs are present. This leads to differences of up to 11% for the lowest aerosol loading observed during the campaign. This effect is most probably caused by the assumed climatology profile of the trace gases, which is not representing the encountered situation correctly. However, even if we use a profile in the model that represents the low aerosol cases, we cannot reproduce the decreasing effect of the aerosols on the photolysis frequencies. The model accounts only for a decrease in $j(O(^1D))$ by aerosols of 10% (AOD 0.1 to 0.4, SZA 20°, see Figure 7), whereas the measurements show a decrease of 33% for DOY 57 (SZA 20°, AOD 0.1) compared to DOY 68 (SZA 20°, AOD 0.4).

[59] Figure 8 shows $j(NO_2)$ versus local solar time for different conditions: clean maritime air above the Indian Ocean, polluted air above the Indian Ocean and polluted air over the eastern United States for comparison. Figure 9 is similar to Figure 8 but plotted versus sec(SZA). The comparison between measured and modeled $j(NO_2)$ show a good agreement for the low aerosol case (DOY 57), but the high aerosol case (AOD = 0.4) is overestimated by the model, even for AOD 0.6. Again the model cannot account for the influence of the aerosol on the photolysis rate. It appears that the absorption of aerosols in the UV is not well parameterized in the LOWTRAN-7 algorithm (Burkert et al., manuscript in preparation, 2002). Within this context, *Jacobson* [1999] hypothesized the absorption of nitrated and aromatic aerosol components and nitrated aromatic gases can play a significant role in the attenuation of the ultraviolet irradiances. In contrast to Figures 8, 9, and 10 show, that $j(NO_2)$ for the low aerosol case is well described

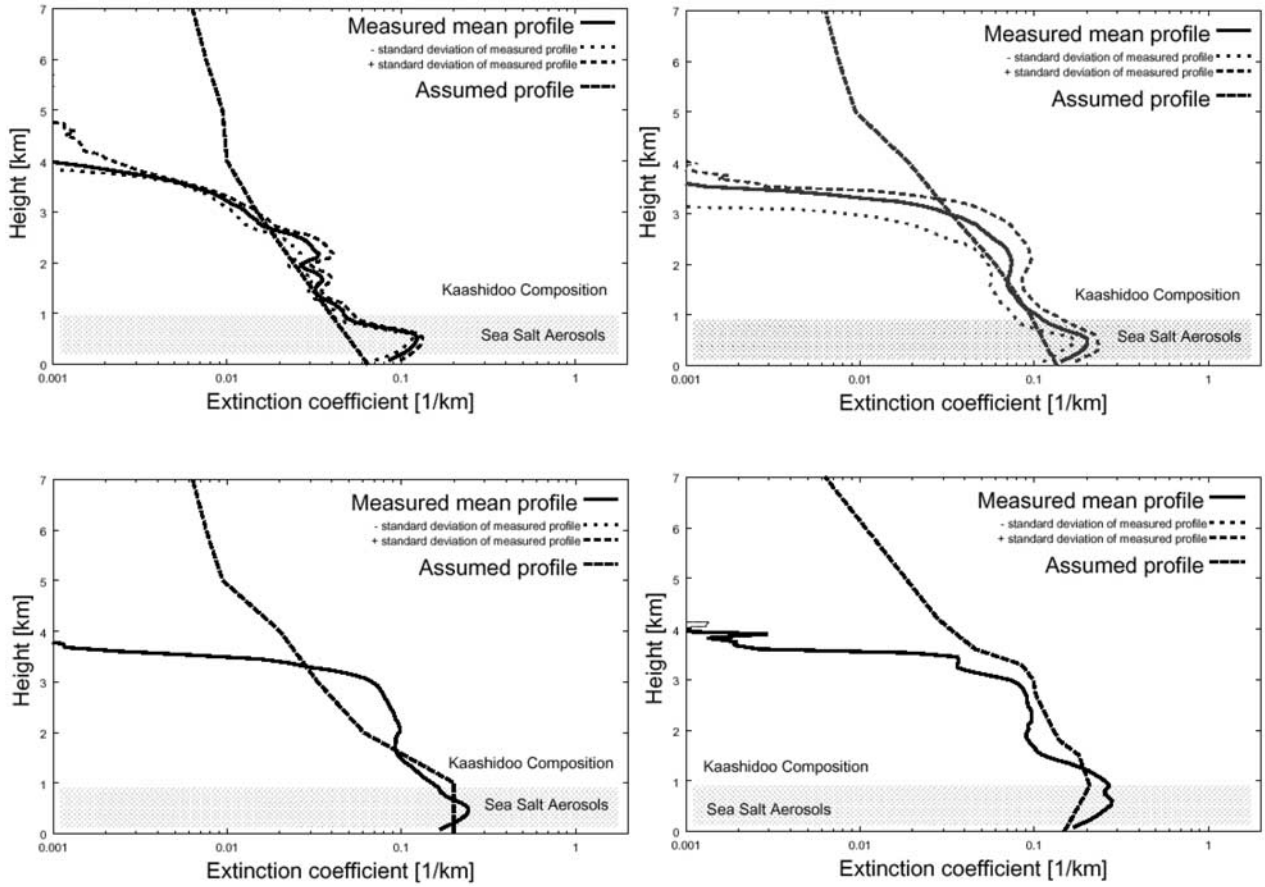

Figure 6. Micropulse lidar (MPL) average profiles for AOD = 0.15, 0.30, 0.45, 0.6. All extinction coefficient profiles are a mixture between the measured and the smooth Lowtran-profile [*Welton et al.*, 2002].

in the model, whereas the high aerosol case is overestimated by ~15%. This different behavior indicates an inaccurate model parameterization in the wavelength behavior of the absorption and/or scattering of the aerosols and/or absorption of nitrated aromatic gases [*Jacobson*, 1999].

[60] Clearly the polluted Indian Ocean air appears to be the most severely impacted by the presence of aerosols. Particles with a low single scattering albedo (ω), as were encountered downwind of India, are more effective at reducing the rate of NO_2 photolysis (and the rate of O_3 production) than are particles having a single scattering albedo near unity, which is the normal situation, encountered over the eastern United States. This is especially true for small solar zenith angles (near solar noon) when enhanced scattered radiation from particles with a high ω compensates for losses in the direct beam. Comparing the $j(NO_2)$ model results with the measurements in Figure 9 shows that the weaker variation with the sec(SZA) for the INDOEX data is well reproduced in the model. Therefore the assumed aerosol composition seems reasonable, only the total amount of absorption by the aerosols is not in agreement with the measured results.

4.2. Interpretation of the INDOEX MBL Chemistry

[61] The chemistry of the MBL during INDOEX was simulated constraining the model to the measurements of trace gases and conditions described above. In more detail, the species, DMS [*Wisthaler et al.*, 2002], H_2 (500 pptv), O_2 (21%), N_2 (78%), CH_4 (1.8 ppmv NH, 1.7 ppmv SH), CO_2 (350 ppmv), NMHC (i.e., C_2H_6, C_3H_8, C_2H_2, C_2H_4, C_3H_6) were held constant in the model. The trace gases, C_2H_2, C_2H_4, and C_3H_6 were fixed to the values measured by (J. Mühle, personal communication, 2002) and are shown in Table 3. These values can only be treated as rough estimates as the probes were partly contaminated by the building up of alkenes due to the long storage time of the canisters (for details, see *Mühle et al.* [2002]). The concentrations can be assumed as upper limits compared with literature values [*Singh and Salas*, 1982; *Duce et al.*, 1983; *Heikes et al.*, 1996]. However, sensitivity studies have shown that the concentration of these species have a negligible influence on the RO_2^* and HCHO model results. The mixing ratios of H_2O, CO, O_3, HCHO [*Wagner et al.*, 2002], and CH_3OH [*Wisthaler et al.*, 2002] were initialized each day with the measured values at 0 UTC. For the trace gases not measured during the cruise, the following values were used for initiation of the photochemistry: H_2O_2 (1000 pptv), and CH_3O_2H (400 pptv). The photolysis frequencies were initialized every 10 min with the values calculated by the PHOTOST model. The model results were scaled to the measured $j(NO_2)$ and $j(O(^1D))$, including the correction for the reflected radiance. No dynamic processes were consid-

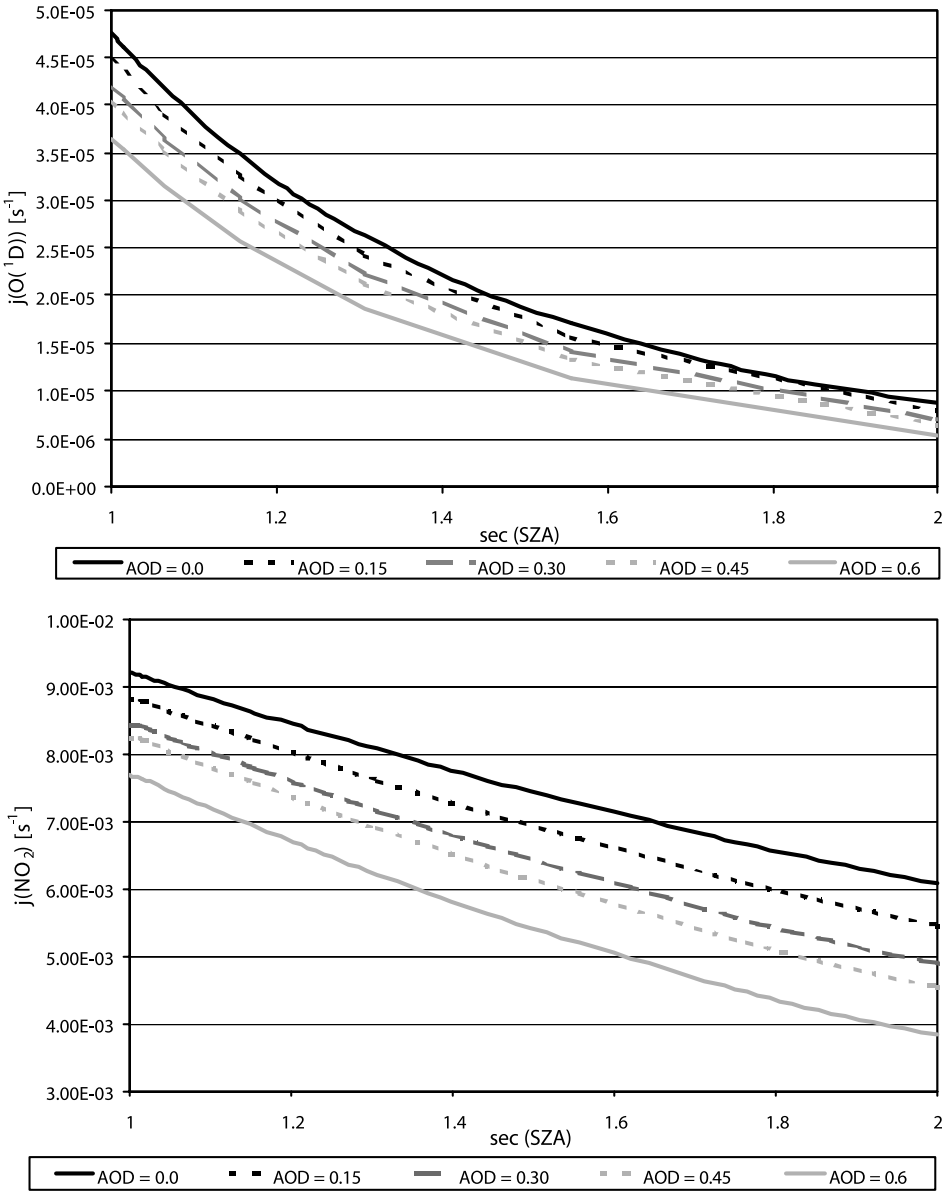

Figure 7. Modeled photolysis frequencies of $j(O(^1D))$ and $j(NO_2)$ for different AOD versus s(SZA).

ered in the box model. Reasonable agreement between simulated and measured trace gases was achieved on most of the days. The analysis of the results highlights the following interesting features:

4.2.1. RO_2^* Diurnal Variation

[62] Figure 11 shows the averaged diurnal behavior for the measured and modeled RO_2^* mixing ratios for the NH and SH. A clear early morning and late afternoon bulge of RO_2^* is observed: The maximum of RO_2^* being around local noon (~UTC +4 hours).

[63] The chemical simulations were performed with two different input values comprising the reported NO for the NH and the SH. In order to achieve reasonable NO behavior, the NO_2 mixing ratio was fixed to either 0 or 10 pptv. In the 10 pptv case, the photodissociation of NO_2 and the reactions between NO, O_3, and NO_2 lead to a diurnal variation of NO with maximum mixing ratios around noon, varying between ~5–8 pptv. Any variation of NO_2 can be neglected, because its reactions are of minor importance for RO_2^* under the investigated conditions.

[64] The averaged maximum RO_2^* mixing ratio, occurring within two hours of local noon, is reasonably well simulated in both hemispheres within the experimental error. Maximum mixing ratios are reached at solar noon. In the SH air masses, the CO mixing ratios are lower than those in the NH air masses, while the amount of CH_4, the dominant hydrocarbon is about the same (SH ~ 1.7 ppmv, NH ~ 1.8 ppmv). As a result, the rate of conversion of OH to HO_2 is reduced and relative to the amount of HO_2 more RO_2, i.e., only organic peroxy radicals without HO_2 are produced. These effect result in the ratio of RO_2 to HO_2 being higher in the SH than in the NH. When small amounts of NO are added to clean NH or SH air in the model, the relative effect

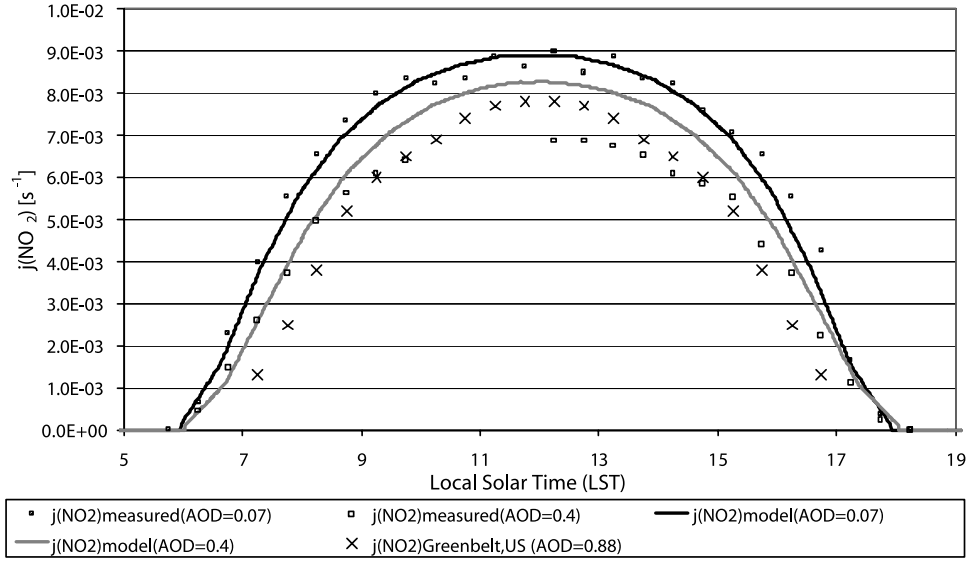

Figure 8. Diurnal variation in the photolysis rate coefficient for NO_2; only cloud-free data are shown. Filled squares (measurements) and the black curve (model) represent data from the clean, marine atmosphere on DOY 57 at 4°S with an AOD of about 0.07 at 500 nm. Open squares (measurements) and gray curve (model) represent data from a polluted atmosphere over the northern Indian Ocean on DOY 65 at 6°N with an AOD of 0.4 at 500 nm. Crosses represent data from the polluted atmosphere over the eastern United States (Greenbelt, Maryland, 39°N) on 15 July 1995 with an AOD of 0.88 at 520 nm and 1.4 at 380 nm.

in the RO_2^* mixing ratio is larger in the SH, because the ratio of RO_2 to HO_2 is larger in the SH than in the NH. A variation of the fixed input NO_2 mixing ratios in the model between 0 and 10 pptv leads to differences in the maximum RO_2^* mixing ratios at noontime up to 20% in the SH and up to 10% in the NH.

[65] The modeled local noontime averaged ratio of RO_2/HO_2 without NO_x chemistry is about 2 for the NH and 3 for

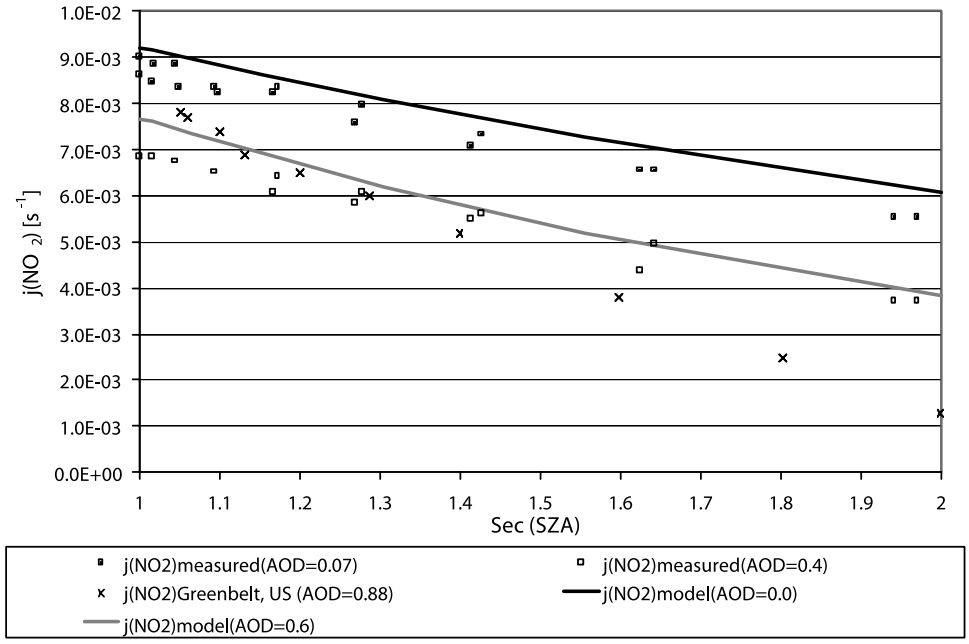

Figure 9. The same data as Figure 8, but with the photolysis rate coefficients plotted as a function of the secant of the solar zenith angle. Filled squares (measurements) and black curve (model) represent data from the clean marine environment; crosses represent data from a polluted environment over North America, and open squares (measurements) and gray curve (model) represent data from a polluted environment in the northern Indian Ocean.

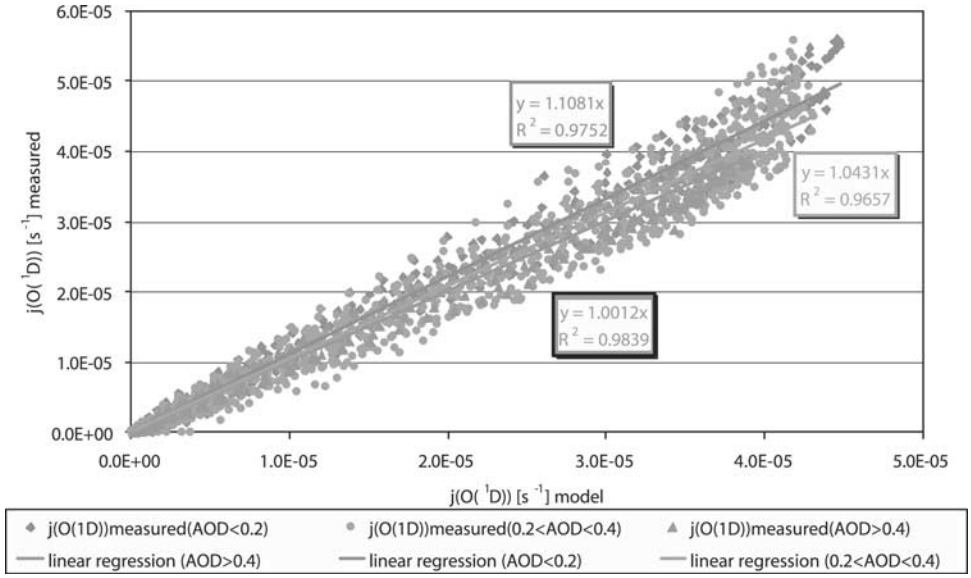

Figure 10. Correlation between measured and modeled j($O(^1D)$ photolysis rates during INDOEX, separated into different AOD ranges. See color version of this figure at back of this issue.

the SH. In the model run with 10 pptv NO_2 the ratio decreases to ~1.6 for the NH and ~1.8 for the SH.

[66] A nonnegligible nocturnal signal of RO_2^* varying between 5 and 10 pptv is observed on most of the days. In contrast the RO_2^* signal decreases to values below the detection limit and close to zero during the occasional rain periods observed during INDOEX. Similar nocturnal signals have been observed previously in the MBL [*Burkert et al.*, 2001b; *Andrés-Hernández et al.*, 2001] and their potential origin has been discussed. According to model investigations, a nocturnal RO_2^* signal of no more than ~3 pptv can be explained. The expected amounts of NO_3 in such remote regions are too low to lead to significant production of RO_2^* through the reactions of NO_3 with VOC during the night. Significant production of radicals by the ozonolysis of alkenes or biogenic species seems also unlikely. The isoprene mixing ratio observed by *Yokouchi et al.* [1999] was generally below 10 pptv above the northern Indian Ocean. This low amount cannot significantly contribute to the production of OH during the night. The ozonolysis of alkenes is also assumed to be negligible due to the low concentrations of light NMHC observed in remote marine regions [*Koppmann et al.*, 1992]. A long-lived RO_2 may explain the observed behavior but its presence is questionable. Such radicals left over from daytime would anyway give decreasing concentrations during nighttime, contrary to the plateau-like signal that is observed.

[67] A likely explanation for the nighttime maritime residual signal of RO_2^* lies in the sensitivity of the PERCA toward ClO_x (Cl + ClO + OClO), reported by *Perner et al.* [1999]. The chain length measured in a PERCA of identical construction to that used during INDOEX has been estimated to be ~300 for dry conditions. As a result the PERCA is about 10 times more sensitive to OClO/ClO than to RO_2^* under the high humidity conditions encountered during the INDOEX campaign, provided that this chain reaction is independent of H_2O. Assuming that this is the origin of the nighttime signal an upper limit of the nighttime ClO/OClO mixing ratio of between 0.3 and 1 pptv is estimated.

[68] There is an ongoing discussion about the presence of halogens in the troposphere. Several mechanisms have been proposed which yield Br_2, BrCl and possibly Cl_2 from inorganic reactions of acidic aerosols [*Sander and Crutzen*, 1996]. Br_2, BrCl and Cl_2 are photolized during daytime and the resulting Br and Cl atoms react with O_3 to form ClO and BrO. ClO reacts with BrO to form OClO. During the day OClO is photolized but at night it is long-lived. Thus the daytime production of relatively small amounts of BrO and ClO might lead to small but significant amounts of OClO at night. No ClO_x measurements were performed during INDOEX. The presence, however, of photochemically produced halogen oxides, in particular iodine oxide in the MBL has been indicated recently by measurements at Mace Head, Ireland [*Carpenter et al.*, 1999].

[69] In early morning and late afternoon the modeled and observed RO_2^* are significantly different. Figure 11 shows that the measured curves of RO_2^* are clearly broader than the simulated diurnal cycles. This effect is less pronounced for the SH. Previous campaigns in the MBL above the Atlantic Ocean have not revealed so clearly such behavior [*Burkert et al.*, 2001b; *Andrés-Hernández et al.*, 2001].

[70] The production of RO_2^* appears to start earlier in the morning and continues longer in the later afternoon than in the model. The broad shape of the RO_2^* diurnal evolution is

Table 3. Assumed Mixing Ratios for C_2H_4, C_3H_6, and C_2H_2 Separated Into Different Air Mass Regions[a]

	C_2H_4	C_3H_6	C_2H_2
SHmT	48	15	20
NHcT	62	22	200
NHcX	60	23	250
NHmT	66	22	25

[a]According to J. Mühle (personal communication, 2002).

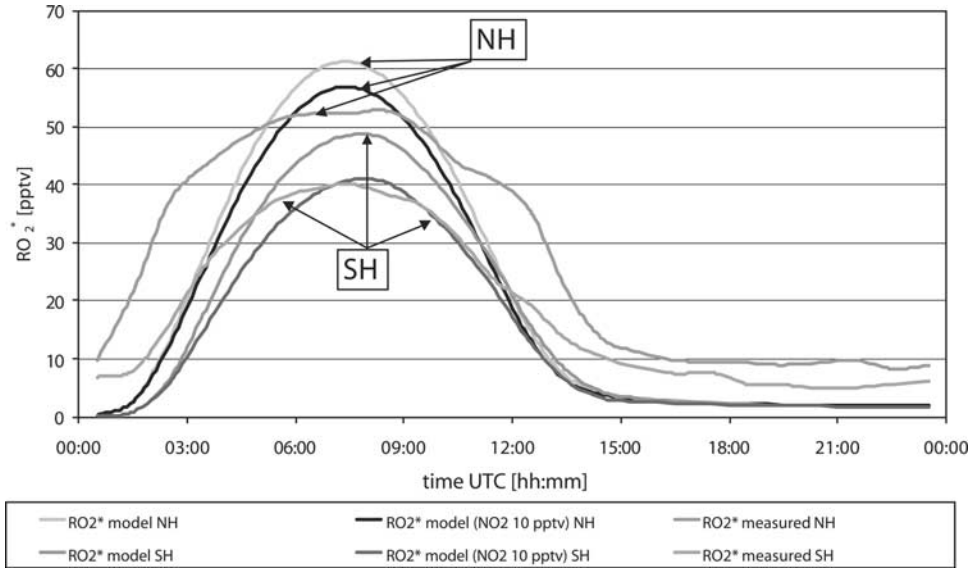

Figure 11. Average diurnal variation of measured and modeled RO_2^* mixing ratios for the NH and SH during INDOEX. Local time is given by UTC + ~4 hours. See color version of this figure at back of this issue.

most pronounced in air parcels originating from India and the Bay of Bengal (see Figure 12). This effect is not correlated with the appearance of higher amounts of NMHC (see Figure 10), but rather with higher amounts of CO, acetone, and HCHO.

[71] Possible explanations for the broad shape behavior or bulge in the morning and evening of the RO_2^* are as follows:

[72] 1. Unidentified VOC: The presence of a "as yet" unidentified VOC having faster reactions rates with OH than either CH_4 and CO, leading to RO_2^* radicals other than

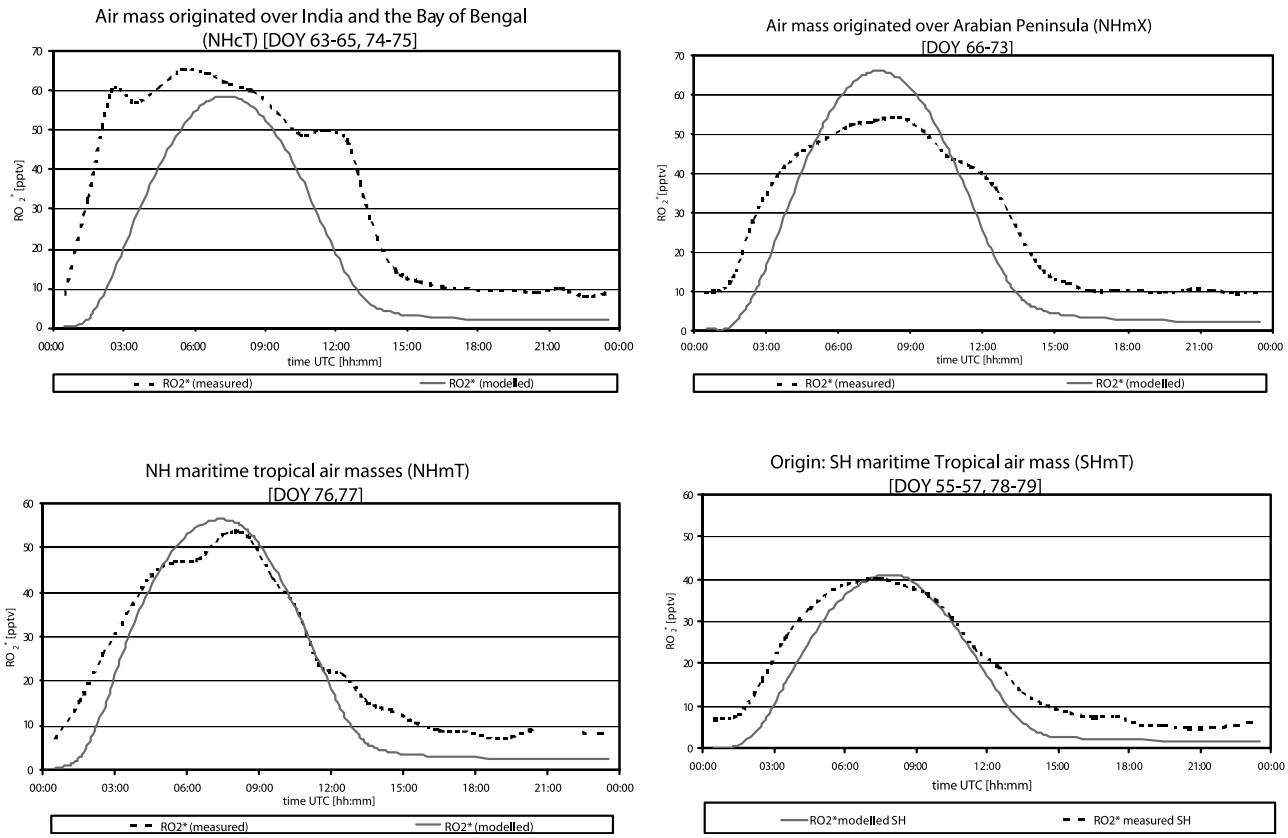

Figure 12. Modeled and measured average diurnal behavior of RO_2^* mixing ratios for different air mass regions during INDOEX. Note: absolute concentrations of measurements and model are in good agreement, but the observations are broader.

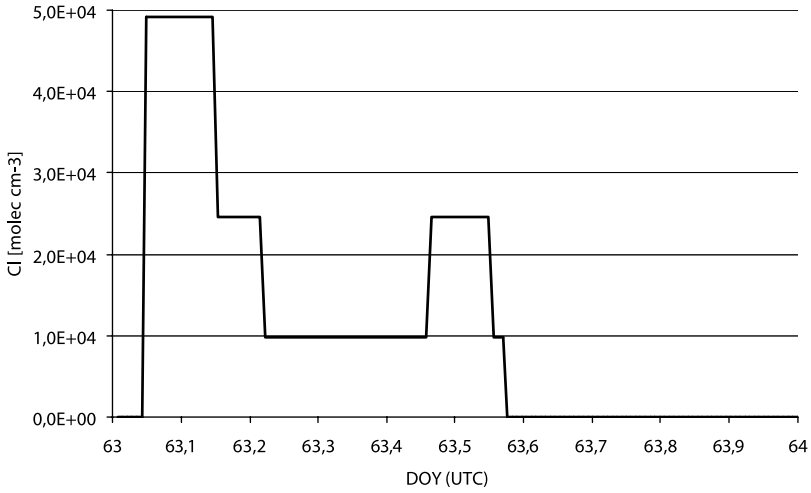

Figure 13. The required diurnal behavior of Cl to describe the observed broad shape in the measured RO_2^* diurnal behavior.

HO_2 and CH_3O_2. The RO_2 additional radical loss reactions also need to be slow compared to the RO_2 reactions considered in the model. This combination of effects would explain the shape of the curve in the early morning and in the evening, but not the flatter plateau at midday.

[73] This further requires that the diurnal variation of this as yet unknown NMHC has a minimum around noon. This implies a short photochemical lifetime, which would prevent such compounds from reaching the open ocean, if emitted by continental sources. Should such a NMHC be emitted from the ocean, the observed NH/SH difference in the RO_2^* diurnal behavior could not readily be explained. Similarly the requirement of having a large source of NMHC is somewhat in conflict with such a compound having a short photochemical lifetime.

[74] 2. Radical reservoir: The presence of a radical reservoir substance, which photolysis in the early morning, producing higher amounts of RO_2^*. This is most likely to be a reservoir for HO_2 radicals, i.e., XHO_2.

$$\begin{aligned} X + HO_2 &\rightarrow HOOX \\ &\vdots \\ HOOX + h\nu &\rightarrow X + HO_2 \end{aligned}$$

[75] The additional reaction of HO_2 with X would lead to smaller amounts of RO_2^* radicals around midday and explain the plateau observed. The consequent reduction of the HO_2/CH_3O_2 ratio implies an increasing lifetime for CH_3O_2 in the evening, which could partly account for the measured nighttime signal. This effect would be more pronounced in the NH due to the higher HO_2/CH_3O_2 ratio, which is a consequence of the higher CO/CH_4 ratio in the NH as compared to the SH.

[76] 3. Bromine and iodine: The presence of the halogen oxides BrO or IO would mean that Br and I atoms are present. These react rapidly with alkenes, alkynes, and aldehydes but not with alkanes. This is, however, an unlikely source of sufficient early morning or late afternoon RO_2^* to explain the bulge. These halogen oxides do react rapidly with both HO_2 and RO_2 and form HOBr and HOI respectively. In the gas phase it is unlikely that sufficient HOBr or HOI is present to explain the bulge in RO_2^*, because this would require relatively large amounts of BrO or IO which would remove O_3.

[77] The presence of halogenoxides like BrO, which react with HO_2 as described in the reactions ((13), (14), and (15)) and lead to a loss of RO_2^*. However, the amounts of halogens needed for the reservoir would unrealistically influence other species, e.g., BrO mixing ratios in the range of a few ppbv would destroy all O_3 present in the MBL.

$$Br + O_3 \rightarrow BrO + O_2 \tag{13}$$

$$BrO + HO_2 \rightarrow BrOH + O_2 \tag{14}$$

$$BrOH + h\nu \rightarrow Br + OH \tag{15}$$

[78] 4. Chlorine. The presence of only small amounts of Cl leads to the oxidation of all VOC, alkanes, alkenes alkynes and thus to an increase of RO_2 radicals. This possible explanation of the bulge in RO_2^* is consistent with the observations of relatively large amounts of HCHO during INDOEX [*Wagner et al.*, 2001, 2002]. The nighttime signal of the PERCA, additionally, provides indirect evidence for the presence of OClO/ClO/Cl in the MBL [*Burkert et al.*, 2001b]. The largest nighttime signals are in regions where the bulge in the diurnal evolution of RO_2^* is most pronounced.

[79] The presence of both chlorine and bromine is predicted to come from sea salt aerosols by the MOCCA model [*Sander and Crutzen*, 1996; *Dickerson et al.*, 1999; *Vogt et al.*, 1996]. Interestingly the diurnal behavior of Cl is different from that of Br: Cl having a maximum in the early morning and late afternoon as required to explain the RO_2^* bulge. The diurnal evolution of Cl, inferred from the RO_2^* observations required to explain the missing source of RO_2^*, is described in Figure 13. This is similar to and in agreement with the diurnal behavior simulated and predicted by the MOCCA model [*Sander and Crutzen*, 1996; R. R. Dickerson et al 2000, personal communication, 2002].

[80] There has been in recent years discussion about the possible presence of a source of Cl in the planetary boundary layer [*Singh et al.*, 1983; *Cicerone*, 1981; *Finlayson-Pitts*, 1993; *Graedel and Keene*, 1995; *Vogt et al.*, 1996; *Moore et al.*, 1996; *Spicer et al.*, 1998; *Yokouchi et al.*, 2000; *Rhew et al.*, 2000; *Keppler et al.*, 2000]. The largest bulge in the diurnal behavior of RO^*_2 was observed in the air masses from India and the surrounding areas of the Bay of Bengal (NHcT). These air masses were characterized by moderate levels of acidity in the aerosols and a moderate nitrate to sulphate ratio [*Ball et al.*, 2003]. The presence of small amounts of NO in these air masses compared to the pristine MBL, would convert ClO to Cl via the reaction:

$$NO + ClO \rightarrow Cl + NO_2, \quad (16)$$

thereby leading to the regeneration of O_3 via the photolysis of NO_2, but enhancing the concentration of Cl. However, concerning the measurements of NO, again the NHcX air masses indicate slightly higher amounts compared to the NHcT air masses (see Table 1).

[81] The measurements of Cl_2 [*Spicer et al.*, 1998] in a coastal region of the eastern USA showed high amounts of Cl_2 during the night, reaching levels up to 150 pptv. Photolysis in the early morning, therefore, produces Cl concentrations of the order of 1.3×10^5 atoms cm^{-3} at maximum. The source of the inorganic Cl_2 is presumably multiphase reactions involving aerosols.

[82] An alternative potential explanation for the presence of higher amounts of Cl in the NHcT regime is the enhanced emissions of halogenated carbon compounds such as CH_3Cl in coastal regions. The oxidation, proceeds in the following mechanism.

$$CH_3Cl + OH \rightarrow CH_2Cl + HCl \quad (17)$$

$$CH_2Cl + O_2 + M \rightarrow CH_2ClO_2 + M \quad (18)$$

$$CH_2ClO_2 + NO \rightarrow CH_2ClO + NO_2 \quad (19)$$

$$CH_2ClO + O_2 \rightarrow CHOCl + HO_2 \quad (20)$$

$$CH_2ClO_2 + HO_2 \rightarrow CH_2ClOOH + O_2 \quad (21)$$

$$CH_2ClO_2 + RO_2 \rightarrow CH_2ClO + RO + O_2 \quad (22)$$

$$CH_2ClO_2 + RO_2 \rightarrow CHOCl + ROH + O_2 \quad (23)$$

$$CH_2ClO_2 + RO_2 \rightarrow CH_2ClOH + R'(R' = R_{H-1})O + O_2 \quad (24)$$

$$CH_2ClOOH + OH \rightarrow CH_2ClO_2 + H_2O \quad (25)$$

$$CH_2ClOOH + OH \rightarrow CHOCl + OH + H_2O \quad (26)$$

$$CH_2ClOOH + h\nu \rightarrow CH_2ClO + OH \quad (27)$$

$$CHOCl + OH \rightarrow CO + Cl + H_2O \quad (28)$$

$$CHOCl + h\nu \rightarrow CO + Cl + H \quad (29)$$

$$CH_2ClOH + OH + O_2 \rightarrow CHOCl + HO_2 + H_2O \quad (30)$$

[83] Several studies [*Khalil and Rasmussen*, 1999; *Moore et al.*, 1996] have shown that the ocean is not a significant source. However, *Yokouchi et al.* [2000] observed up to 2100 pptv of CH_3Cl on islands in the tropics. It is not clear, if these high mixing ratios are related to emissions from the forested land.

[84] An upper limit of Cl mixing ratio generated from 2100 pptv of CH_3Cl can be calculated by a simple steady state assumption for Cl and the hypothesis that every CH_3Cl oxidized by OH leads to a Cl.

$$[Cl] = \frac{k_{CH_3Cl+OH}[CH_3Cl][OH]}{k_{CH_4+Cl}[CH_4]} \quad (31)$$

[85] This yields [Cl] = 5.9×10^3 [atoms cm^{-3}], for an [OH] = 1×10^7 [molecule cm^{-3}] and mixing ratio of CH_4 = 1.8 ppmv, i.e., apparently too small to explain the observed effect. In addition, the measurements of CH_3Cl onboard the citation plane during INDOEX only indicated amounts in the NHcT air masses of up to 750 pptv [*Scheeren et al.*, 2002].

[86] Overall, the nighttime RO^*_2 signals and the bulge in RO^*_2 appears to provide evidence for a source of Cl in the MBL, which maximizes in the early morning. This source is most likely to comprise inorganic multiphase reactions on sea salt aerosol, but the oxidation of organic halides cannot be excluded.

4.2.2. Assessment of the Contribution of Cl to the Tropospheric Oxidising Capacity (OC) of CH_4

[87] The OC with respect to oxidation and consequent removal of a species from the marine boundary layer can be defined as the sum of the effective first-order reactive removal processes.

$$OC_{CH_4} = \int_{day} (k_{OH+CH_4}[OH][CH_4] + k_{Cl+CH_4}[Cl][CH_4])dt$$

[88] Assuming that the bulge in RO^*_2 results from Cl, and this indicates that above the Indian Ocean Cl accounts for up to ~8% of the average oxidizing capacity of CH_4. A daily integral was chosen to compare the OC of OH and Cl. The Cl diurnal profile was the same as presented in Figure 13.

4.2.3. Comparison of the Remote MBL Above the Atlantic and Indian Ocean

[89] The average RO^*_2 behavior from the measurements made in the NH and SH in the Atlantic Ocean are shown in Figures 14 and 15. These measurements were made during the ALBATROSS campaign in 1996 [*Burkert et al.*, 2001b] and AEROSOL in 1999, immediately prior to INDOEX with the same instrument [*Andrés Hernández et al.*, 2001].

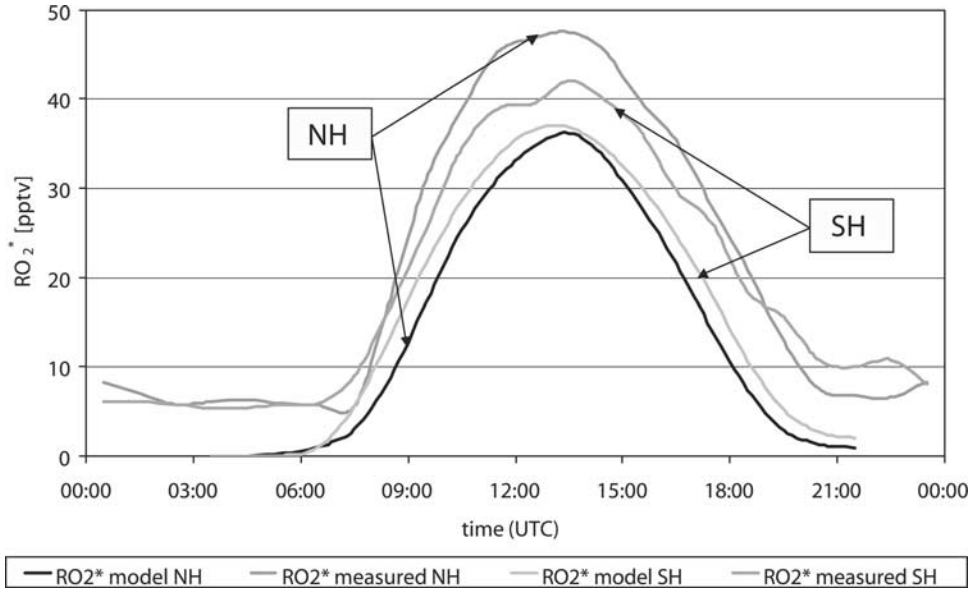

Figure 14. Average diurnal variation of measured and modeled RO_2^* mixing ratios for the NH and SH during ALBATROSS (1996) above the Atlantic Ocean. Local time is given by UTC + ~2 hours. See color version of this figure at back of this issue.

The ALBATROSS cruise went aboard the Polarstern from Bremerhaven, Germany (54°N, 9°E) to Punta Quilla, Argentina (50°S, 67°W). Much of the voyage was around 30°W with the Polarstern traveling from north to south. In contrast the AEROSOL cruise went from Norfolk, Virginia (37°N, 76°W) to Cape Town, South Africa (34°S, 22°E), cutting across the North and South Atlantic Oceans.

[90] Using the measured amounts of O_3 and related trace gases and neglecting any halogen chemistry, the model predicts similar concentrations of RO_2^* in both the NH and the SH in both 1996 and 1999: the noontime maximum mixing ratio of RO_2^* being around 36 pptv. In contrast the estimated amounts of RO_2^* in the northern and southern part so the Indian Ocean are significantly different.

[91] The measurements from the Atlantic Ocean show for both the ALBATROSS and the AEROSOL campaign the following:

[92] 1. The broader shape behavior is more pronounced in the NH than in the SH.

[93] 2. The noontime maximum of RO_2^* is small but significantly higher in the NH than in the SH.

[94] 3. The early morning increase of RO_2^* is not as fast as in the results from the Indian Ocean.

[95] 4. The broader shape in the Atlantic Ocean results appears similar to an offset throughout the day.

[96] 5. The nighttime unexplained signal is not considered to be an artifact of the PERCA, because during periods of rain the signal was observed to go zero both during the day and night.

[97] The differences between the Atlantic and the Indian Ocean are most probably caused by the presence of higher amounts of NO_x, CO, and NMHC, different meteorological conditions (i.e., higher MBL height in the Atlantic compared to the Indian Ocean). The diurnal behavior of the O_3 mixing ratio above the Atlantic Ocean does not often show significant loss of O_3. This is another indication for production of O_3 from the higher amounts of NO_x although the measurements above the Atlantic Ocean were performed far away from coastal regions. In addition, the difference in the O_3 mixing ratio between NH and SH is small above the Atlantic Ocean during the ALBATROSS and AEROSOL campaign.

[98] The MBL of the remote Indian Ocean seems generally to be cleaner than the remote parts of the Atlantic Ocean visited on the research voyages and exhibits the cleanest air observed thus far in the SH. This may explain why the behavior of the small amounts of halogens has a more pronounced effect on the RO_2^*.

[99] The RO_2^* and HCHO chemistry are closely related in the MBL. The production of alkoxy, RO, radicals from peroxy radicals leads to the production of aldehydes and ketones via the reactions of RO with O_2: the reaction of CH_3O with O_2 is expected to be the main source of HCHO in the remote MBL. The photolysis of HCHO is an additional significant source of HO_2 radicals in the MBL as compared with the reaction of OH with CO in the presence of O_2.

[100] It has been reported in the past, that measured HCHO concentrations in the MBL of the Atlantic Ocean are in disagreement with model results [*Burkert et al.*, 2001b; *Weller et al.*, 2000, and references therein]. This has been attributed to additional sources of nonmethane hydrocarbons, e.g., from ship exhaust and biomass burning plumes crossing the ocean [*Burkert et al.*, 2001b].

[101] The HCHO expected in the MBL above the Indian Ocean was simulated using the chemical model and compared with the measurements performed during INDOEX. As for RO_2^* simulations, the NO_2 was constrained to fixed amounts of either 0 or 10 pptv, which represent the minimum and maximum in the range of observations.

[102] In regions exhibiting low CO values, the effect of NO_x on the amount of HCHO is more pronounced due to the higher rate of conversion of RO_2 radicals to HO_2. As a result, the NO_2 values used in the model determine to a large extent the calculated HCHO mixing ratio. In Figure 16 the daily averages of measured and calculated HCHO

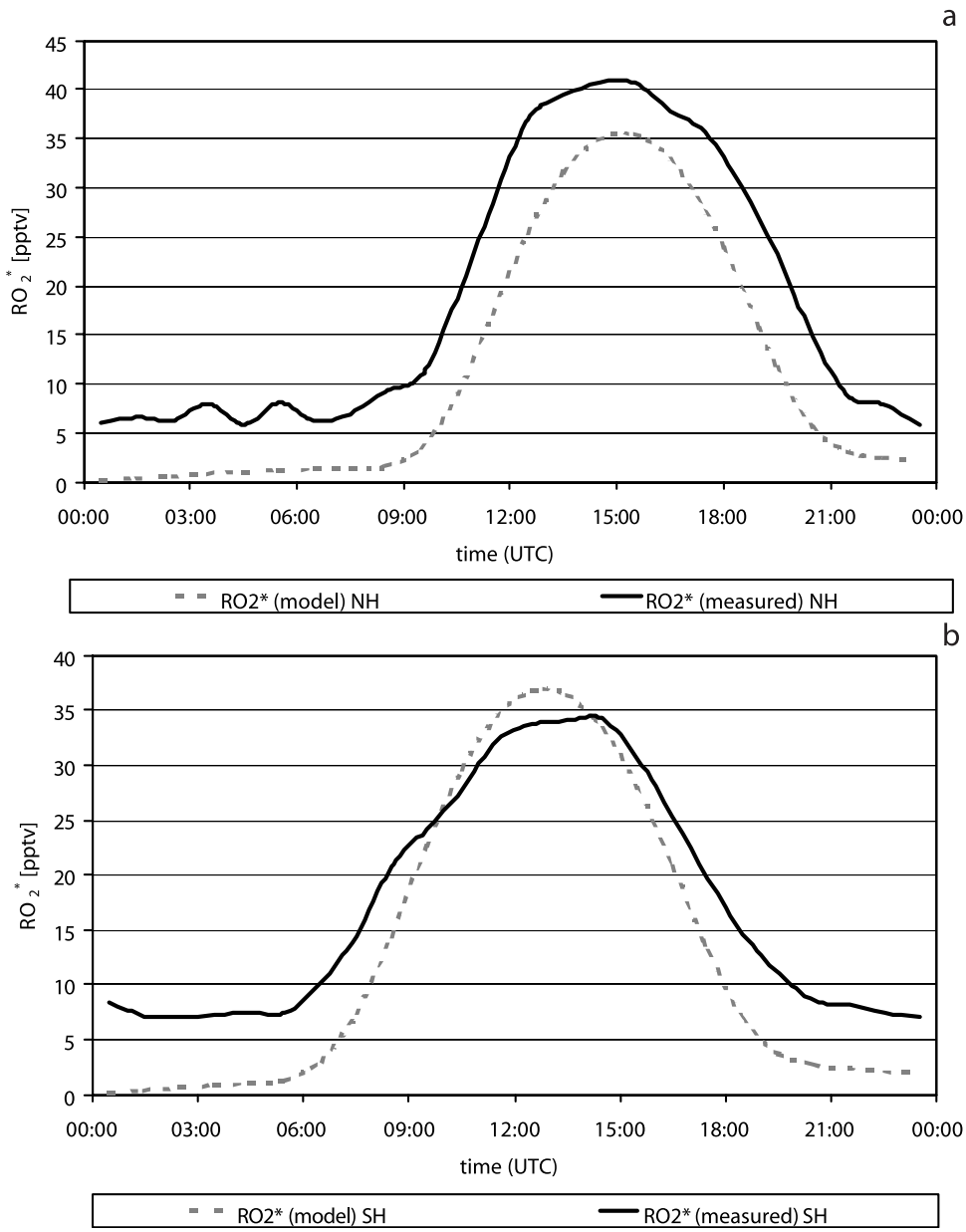

Figure 15. Average diurnal variation of measured and modeled RO_2^* mixing ratios for the (a) NH and (b) SH during AEROSOL (1999) above the Atlantic Ocean. Local time approximately UTC (a) +4 hours and (b) +2 hours.

mixing ratios are plotted. In spite of the uncertainty in the NO measurements mentioned above, the agreement is fair between measured and simulated HCHO, taking the experimental error into account. This is similar to the results obtained by *Wagner et al.* [2001].

[103] In the period DOY 68–70 the simulated HCHO values are significantly larger than the measured amounts. This is similar to previous results [*Liu et al.*, 1992; *Jacob et al.*, 1996]. Some investigators have proposed that the heterogeneous chemistry in clouds or aerosols as being responsible for the fast loss of HCHO. On those days, where this behavior is observed however, the AOD measured is lower than on previous days.

[104] An alternative explanation of the low HCHO mixing ratios has been recently reported by *Wagner et al.* [2001]. For this explanation, the lower HCHO mixing ratios are interpreted to be an indication of the prevailing free tropospheric character of the subsiding air measured. The back trajectories of the air masses in this case, however, indicate that the air sampled on the days in question remained for at least two days in the MBL, which is sufficient time for HCHO to achieve a stationary state.

[105] The observed relationship between the daily maximum measured mixing ratios of CO, HCHO, and RO_2^* confirm the close chemical link between these species. The model results cannot explain the extremely high concentrations of RO_2^* observed during the DOY 64 and 65. Surprisingly during days with enhanced levels of NMHC (DOY 68–72) no enhanced RO_2^* or HCHO mixing ratios are observed.

[106] For enhanced CO levels (DOY 63–65) and maximum noontime RO_2^* mixing ratios, the model does not reproduce the observed HCHO values. In the model higher

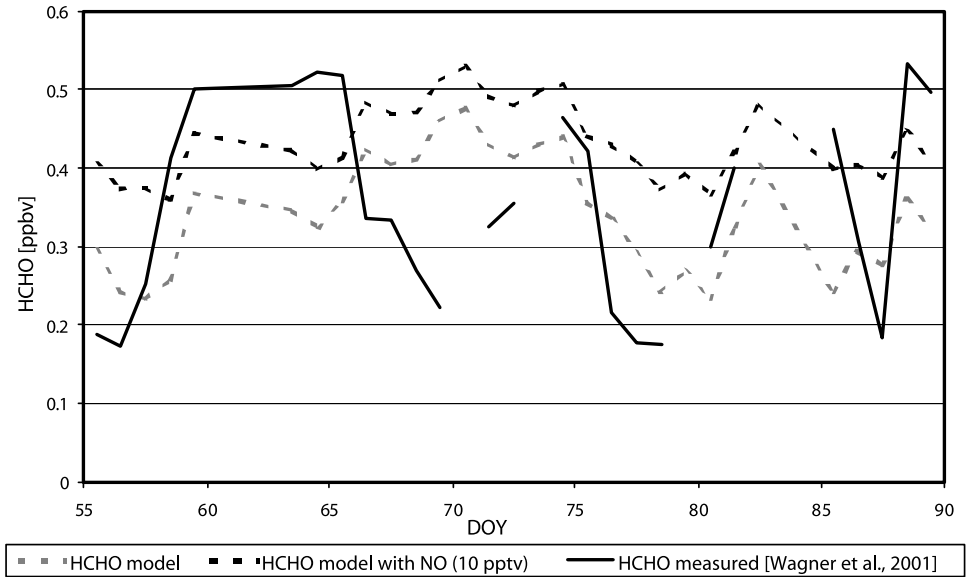

Figure 16. Measured and modeled HCHO mixing ratios during INDOEX.

CO concentrations lead to higher HO_2 and less OH. This results in a lower production rate of CH_3O_2 via the oxidation of methane and also a higher loss rate as a result of the HO_2 reaction with CH_3O_2. The CH_3O_2 loss reactions are the main source for HCHO. Under the assumption that all other radical sources do not significantly increase, then for higher CO concentrations it is difficult to explain the CO and HCHO correlation observed, because the opposite effect is predicted from the expected chemistry.

[107] Possible explanations of the HCHO behavior:

[108] 1. A reaction of CO and OH in the presence of water producing HCHO via a complex mechanism, e.g.,

$$CO + OH \rightarrow COOH$$
$$COOH + H_2O \rightarrow HCHO + HO_2$$

[109] However, this reaction is expected to be slow and is endoergic.

[110] 2. A reaction of CO and HO_2 catalyzed by the presence of water, which produces OH and CO_2. Some studies in the past have indicated that their reaction may occur but other have obtained a very low upper limit for this reaction rate coefficient [*DeMore et al.*, 1997, and references therein]. However, an extended investigation concerning the influence of water on the reaction rate coefficient has not yet been done. A reaction of the described type would change the ratio between HO_2 and OH and would also increase the amount of RO_2 due to the higher amount of OH present. Such a reaction would lead via enhanced OH concentrations to an enhanced oxidation of hydrocarbons and rate of production of RO_2 and consequently to a larger production of HCHO in the atmosphere.

[111] 3. The presence of a NMHC, which has not yet been identified and included in the model having similar sources to CO. Its rate of oxidation needs to be in the same order of magnitude to that of CH_4.

[112] 4. The presence of another oxidizing agent like OH for example Cl, which leads to additional amounts of RO_2^* and therefore higher concentrations of HCHO. This requires amounts of Cl to be in the order of 1×10^4 to 1×10^5 molecules cm^{-3}.

[113] It is very interesting to note that measurements of the isotopic fractionation of CH_4 above the Pacific Ocean have recently provided evidence for the enrichment of the CH_4 fractions, which cannot be explained by OH chemistry alone. An additional oxidant is required [*Allan et al.*, 2001].

[114] In summary it is probably far from surprising that the broad shape behavior of RO_2^* is coincidental with increased amounts of HCHO in the INDOEX measurements. The oxidation of CH_4 and for that matter any other NMHC, initiated by Cl would in pristine regions of the atmosphere yield additional HCHO, compared to that predicted from the OH initiated CH_4 and NMHC oxidation in the remote pristine atmosphere.

[115] Finally assuming that the bulge in RO_2^* results from Cl, and this indicates that in the remotes and pristine Cl accounts for up to ~8% of the average oxidizing capacity of CH_4 of the atmosphere.

5. Summary

[116] A set of trace gases and photolysis frequencies have been successfully measured in the MBL above the Indian Ocean during the INDOEX campaign in February, March, and April 1999. Air masses with different trace gas mixing ratios and origin have been encountered and analyzed.

[117] The photolysis frequencies at the ground level were calculated using an RTM and compared with measured values. The model was initialized with the measured AOD profiles and aerosol composition. The $j(O(^1D))$ and $j(NO_2)$ calculated photolysis frequencies at 30° SZA for AOD of 0 and 0.6 differ by about 30% and 24% respectively.

[118] A box homogenous gas phase chemistry model has been used to simulate the chemistry of the MBL and its results compared with the trace gas and radical measurements. The diurnal behavior of the measured RO_2^* is observed to be significantly broader than that estimated using an OH oxidation scheme suitable for the pristine and

remote MBL. This broad RO_2^* or bulge behavior indicates that more RO_2^* is present in the early morning and late afternoon than OH chemistry predicts.

[119] The presence of the broader RO_2^* behavior is not correlated with the amount of NMHC but can be related to the origin of the air masses. Overall this behavior indicates the presence of missing chemistry in the model in the early morning and late afternoon. One reasonable explanation of the observed behavior is the presence of small amounts chlorine in the MBL. The sources of Cl are most likely to be the release from aerosols and also possibly the oxidation of organic halides.

[120] The agreement between the modeled and measured HCHO is reasonable taking the experimental error and the uncertainty of NO measurements into account. The observed relationship between the daily measured maximum mixing ratios of CO, HCHO, and RO_2^* indicates a close chemical link between these species, which cannot be well explained by the known OH oxidation chemistry used in the box model. The most likely explanation of this behavior is the presence of Cl in the MBL, as proposed above.

[121] Overall the measurements of trace gases and radicals, obtained aboard the R/V *Ronald H. Brown* during INDOEX have provided the first detailed observations of the chemistry of the remote marine boundary layer above the Indian Ocean. The observed RO_2^* is not that expected for OH initiated hydrocarbon oxidation. Evidence is presented, which indicates that Cl contributes significantly to the oxidative capacity of the tropical MBL. To gain confidence about the proposed explanation of the RO_2^* behavior, research campaigns focusing on the identification of halogen oxide radicals in the MBL are required.

[122] **Acknowledgments.** We would like to thank all participants of the INDOEX campaign for their valuable data, especially Volker Wagner et al. for their HCHO data. The initiators of INDOEX deserve an extra mention. Special thanks are extended to the crew of the research vessel Ronald H. Brown, without whose assistance. This study was in part funded by the University of Bremen, the EU PRIME project, and the German Ministry of Science and Education (BMBF) and the German Space Agency (DLR). The RRD was supported by NSF ATM-9612893.

References

Allan, W., D. C. Lowe, and J. M. Cainey, Active chloride in the remote marine boundary layer: Modeling anomalous measurements of δ13C in methane, *Geophys. Res. Lett.*, *28*(17), 3239–3242, 2001.

Andrés-Hernández, M. D., J. Burkert, L. Reichert, D. Stöbener, J. Meyer-Arnek, R. R. Dickerson, B. G. Doddridge, and J. P. Burrows, Marine boundary layer peroxy radical chemistry during the AEROSOLS99 campaign: Measurements and analysis, *J. Geophys. Res.*, *106*(18), 20,833–20,846, 2001.

Atkinson, R., D. L. Baulch, R. A. Cox, R. F. Hampson, J. A. Kerr, M. J. Rossi, and J. Troe, Evaluated kinetic and photochemical data for atmospheric chemistry, IUPAC subcommittee on gas kinetic data evaluation for atmospheric chemistry, *J. Phys. Chem.. Ref. Data.*, *29*, (suppl. VIII), 167–266, 2000.

Ball, W. P., R. R. Dickerson, B. G. Doddridge, J. Stehr, T. Miller, D. Savoie, and T. P. Carsey, Bulk and size-segregated aerosol composition observed during INDOEX 1999: Overview of meteorology and continental impacts, *J. Geophys. Res.*, *108*, doi:10.1029/2002JD002467, in press, 2003.

Blindauer, C., V. Rozanov, and J. P. Burrows, Actinic flux and photolysis frequency comparison computations using the model PHOTOGT, *J. Atmos. Chem.*, *24*, 1–21, 1996.

Bruehl, C., and P. J. Crutzen, MPIC Two-dimensional model, in *The Atmospheric Effects of Stratospheric Aircraft*, *NASA Ref. Publ. 1292*, pp. 103–104, NASA, Greenbelt, Md., 1993.

Buchwitz, M., A correlated-k distribution scheme for overlapping gases suitable for retrieval of atmospheric constituents from moderate resolution radiance measurements in the visible/near-infrared spectral region, *J. Geophys. Res.*, *105*(12), 15,247–15,261, 2000.

Burkert, J., T. Behmann, M. D. Andrés-Hernández, D. Stöbener, M. Weißenmeyer, D. Perner, and J. P. Burrows, Measurements of peroxy radicals in a forested area of Portugal, chemosphere, *Global Change Sci.*, *3*, 327–338, 2001a.

Burkert, J., M.-D. Andrés-Hernández, D. Stöbener, J. P. Burrows, M. Weissenmayer, and A. Kraus, Peroxy radical and related trace gas measurements in the boundary layer above the Atlantic Ocean, *J. Geophys. Res.*, *106*(6), 5457–5477, 2001b.

Burrows, J. P., et al., The global ozone monitoring experiment (GOME): Mission concept and first scientific results, *J. Atmos. Sci.*, *56*, 151–175, 1999.

Bush, B. C., and F. P. J. Valero, Spectral aerosol radiative forcing at the surface during the Indian Ocean Experiment (INDOEX), *J. Geophys. Res.*, *107*(D19), 8003, doi:10.1029/2000JD000020, 2002.

Carpenter, L. J., W. T. Sturges, S. A. Penkett, P. S. Liss, B. Alicke, K. Hebestreit, and U. Platt, Short-lived alkyl iodides and bromides at Mace Head, Ireland: Links to biogenic sources and halogen oxide production, *J. Geophys. Res.*, *104*(D1), 1679–1690, 1999.

Carroll, M. A., M. McFarland, B. A. Ridley, and D. L. Albritton, Ground-based nitric oxide measurements at Wallops Island, Virginia, *J. Geophys. Res.*, *90*, 12,853–12,860, 1985.

Carsey, T. P., D. D. Churchill, M. L. Farmer, C. J. Fischer, A. A. Pszenny, V. B. Ross, E. S. Saltzman, M. Springer-Young, and B. Bonsang, Nitrogen oxides and ozone production in the North Atlantic marine boundary layer, *J. Geophys. Res.*, *102*, 10,653–10,665, 1997.

Carver, G. D., P. D. Brown, and O. Wild, The ASAD atmospheric chemistry integration package and chemical reaction database, *Comput. Phys. Commun.*, *105*, 197–215, 1997.

Cicerone, R. J., Halogens in the atmosphere, *Rev. Geophys. Space Phys.*, *19*, 123–139, 1981.

Clemitshaw, K. C., L. J. Carpenter, S. A. Penket, and M. E. Jenkin, A calibrated peroxy radical chemical amplifier (PERCA) instrument for ground-based tropospheric measurements, *J. Geophys. Res.*, *102*, 25,405–25,416, 1997.

Cox, C., and W. Munk, Measurement of the roughness of the sea surface from photographs of the sun's glitter, *J. Opt. Soc. Am.*, *44*, 838–850, 1954.

Crutzen, P. J., A discussion of the chemistry of some minor constituents in the stratosphere and troposphere, *Pure Appl. Geophys.*, *106–108*, 1385–1399, 1973.

Crutzen, P. J., and V. Ramanathan, Foreword, *J. Geophys. Res*, *106*(D22), 28,369–28,370, 2001.

DeMore, W. B., S. P. Sander, D. M. Golden, R. F. Hampson, M. J. Kurylo, C. J. Howard, A. R. Ravishankara, C. E. Kolb, and M. J. Molina, Chemical kinetics and photochemical data for use in stratospheric modeling, *JPL Eval. 12*, Jet Propul. Lab., Pasadena, Calif., 1997.

Dickerson, R. R., and A. C. Delany, Modification of a commercial gas filter correlation CO detector for increased sensitivity, *J. Atmos. Oceanic Technol.*, *5*(3), 424–431, 1988.

Dickerson, R. R., K. P. Rhoads, T. P. Carsey, S. J. Oltmans, J. P. Burrows, and P. J. Crutzen, Ozone in the remote marine boundary layer: A possible role for halogens, *J. Geophys. Res.*, *104*, 21,385–21,395, 1999.

Dickerson, R. R., M. O. Andreae, T. Campos, O. L. Mayol-Bracero, C. Neususess, and D. G. Streets, Analysis of black carbon and carbon monoxide observed over the Indian Ocean: Implications for emissions and photochemistry, *J. Geophys. Res.*, *107*(D19), 8017, doi:10.1029/2001JD000501, 2002.

Duce, R. A., V. A. Mohnen, P. R. Zimmermann, D. Grosjean, W. Cautreels, R. Chatfield, R. Jaenicke, J. A. Ogren, E. D. Pellizzari, and G. T. Wallace, Organic material in the global troposphere, *Rev. Geophys. Space Phys.*, *21*(4), 921–952, 1983.

Finlayson-Pitts, B. J., Chlorine atoms as a potential tropospheric oxidant in the marine boundary layer, *J. Res. Chem. Intermed.*, *19*, 235–249, 1993.

Graedel, T. E., and W. C. Keene, The tropospheric budget of reactive chlorine, *Global Biogeochem. Cycles*, *9*, 47–77, 1995.

Hastie, D. R., M. Weißenmayer, J. P. Burrows, and G. W. Harris, Calibrated chemical amplifier for atmospheric ROx measurements, *Anal. Chem.*, *63*, 2048–2057, 1991.

Heikes, B., M. Lee, D. Jacob, R. Talbot, J. Bradshaw, H. Singh, D. Blake, B. Anderson, H. Fuelberg, and A. M. Thompson, Ozone, hydroperoxides, oxides of nitrogen, and hydrocarbon budgets in the marine boundary layer over the South Atlantic, *J. Geophys. Res.*, *101*(D19), 24,221–24,234, 1996.

Hofzumahaus, A., A. Kraus, and M. Müller, Solar actinic flux spectroradiometry: A technique for measuring photolysis frequency in the atmosphere, *Appl. Opt.*, *21*, 4443–4460, 1999.

Jacob, D. J., et al., Origin of ozone and NOx in the tropical troposphere: A photochemical analysis of aircraft observations over the South Atlantic basin, *J. Geophys. Res.*, *101*, 24,235–24,250, 1996.

Jacobson, M. Z., Isolating nitrated and aromatic aerosols and nitrated aromatic gases as sources of ultraviolet light absorption, *J. Geophys. Res.*, *104*(D3), 3527–3542, 1999.

Jin, Z., T. Charlock, and K. Rutledge, Analysis of broadband solar radiation and albedo over the ocean surface at COVE, *J. Atmos. Oceanic Technol.*, *19*(10), 1585–1601, 2002.

Junkermann, W., U. Platt, and A. Volz-Thomas, A photoelectric detector for the measurement of photolysis frequency of ozone and other atmospheric molecules, *J. Atmos. Chem.*, *8*, 203–227, 1989.

Kelley, P., R. R. Dickerson, W. T. Luke, and G. L. Kok, Rate of NO2 photolysis from the surface to 7.6 km altitude in clear sky and clouds, *Geophys. Res. Lett.*, *22*(19), 2621–2624, 1995.

Keppler, F., R. Eiden, V. Niedan, J. Pracht, and H. F. Schöler, Halocarbons produced by natural oxidation processes during degradation of organic matter, *Nature*, *403*, 298–301, 2000.

Khalil, M. A. K., and R. A. Rasmussen, Atmospheric methyl chloride, *Atmos. Environ.*, *33*, 1305–1321, 1999.

Koppmann, R., R. Brauers, F. J. Johen, C. Plass, and J. Rudolph, The distribution of light nonmethane hydrocarbons over the mid-Atlantic: Results of the Polarstern Cruise ANT VII/1, *J. Atmos. Chem.*, *15*, 215–234, 1992.

Lelieveld, J., et al., The Indian Ocean Experiment: Widespread air pollution from South and Southeast Asia, *Science*, *291*, 1031–1036, 2001.

Levy, H., II, Normal atmosphere: Large radical and formaldehyde concentrations predicted, *Science*, *173*, 141–143, 1971.

Lightfoot, P. D., R. A. Cox, J. N. Crowley, M. Destriau, G. D. Hayman, M. E. Jenkin, G. K. Moortgat, and F. Zabel, Organic peroxy radicals: Kinetics, spectroscopy and tropospheric chemistry, *Atmos. Environ., Part A*, *26*, 1805–1951, 1992.

Liu, S. C., et al., A study of the photochemistry and ozone budget during the Mauna Loa Observatory Photochemistry Experiment, *J. Geophys. Res.*, *97*, 10,463–10,471, 1992.

Meywerk, J., and V. Ramanathan, Observations of the spectral clear-sky aerosol forcing over the tropical Indian Ocean, *J. Geophys. Res.*, *104*, 24,359–24,370, 1999.

Meywerk, J., and V. Ramanathan, Influence of anthropogenic aerosols on the total and spectral irradiance at the sea surface during the Indian Ocean Experiment (INDOEX) 1999, *J. Geophys. Res.*, *107*(D19), 8018, doi:10.1029/2000JD000022, 2002.

Mihele, C. M., and D. R. Hastie, The sensitivity of the radical amplifier to ambient water vapor, *Geophys. Res. Lett.*, *25*, 1911–1913, 1998.

Moore, R. M., W. Groszko, and S. J. Niven, Ocean-atmosphere exchange of methyl chloride: Results from NW Atlantic and Pacific Ocean studies, *J. Geophys. Res.*, *101*, 28,529–28,539, 1996.

Mühle, J., A. Zahn, C. A. M. Brenninkmeijer, V. Gros, and P. J. Crutzen, Air mass classification during the INDOEX R/V *Ronald Brown* cruise using measurements of nonmethane hydrocarbons, CH_4, CO_2, CO, ^{14}CO, and $\delta^{18}O(CO)$, *J. Geophys. Res.*, *107*(D19), 8021, doi:10.1029/2001JD000730, 2002.

Neusüß, C., T. Gnauk, A. Plewka, H. Herrmann, and P. K. Quinn, Carbonaceous aerosol over the Indian Ocean: OC/EC fractions and selected specifications from size-segregated onboard samples, *J. Geophys. Res.*, *107*(D19), 8031, doi:10.1029/2001JD000327, 2002.

Parsons, R. L., and R. R. Dickerson, NOAA Ship Ronald H. Brown: World global climate study, *Sea Technol.*, *40*, 39–45, 1999.

Perner, D., T. Arnold, J. Crowley, T. Klüpfel, M. Martinez, and R. Seuwen, The measurement of active chlorine in the atmosphere by chemical amplification, *J. Atmos. Chem.*, *34*, 2–9, 1999.

Quinn, P. K., D. J. Coffman, T. S. Bates, T. L. Miller, J. E. Johnson, E. J. Welton, C. Neusüss, M. Miller, and P. J. Sheridan, Aerosol optical properties during INDOEX 1999: Means, variability, and controlling factors, *J. Geophys. Res.*, *107*(D19), 8020, doi:10.1029/2000JD000037, 2002.

Ramanathan, V., et al., Indian Ocean Experiment: An integrated analysis of the climate forcing and effects of the great Indo-Asian haze, *J. Geophys. Res.*, *106*(D22), 28,371–28,398, 2001.

Reichert, L., Untersuchung des Wassereffektes eines Peroxyradikal-Detektors, M.S. thesis, Univ. of Bremen, Bremen, Germany, Apr. 2000.

Reichert, L., M. D. Andrés Hernández, D. Stöbener, J. Burkert, and J. P. Burrows, Investigation of the effect of water complexes in the determination of peroxy radical ambient concentrations: Implications for the atmospheres, *J. Geophys. Res.*, *108*(D1), 4017, doi:10.1029/2002JD002152, 2003.

Rhew, R. C., B. R. Miller, and R. F. Weiss, Natural methyl bromide and methyl chloride emissions from coastal salt marshes, *Nature*, *403*, 292, 2000.

Rhoads, K., P. Kelley, R. R. Dickerson, T. P. Carsey, M. Farmer, D. Savoie, and J. Prospero, The composition of the troposphere over the Indian Ocean during the monsoonal transition, *J. Geophys. Res.*, *102*, 18,981–18,995, 1997.

Rozanov, V. V., T. Kurosu, and J. P. Burrows, Retrieval of atmospheric constituents in the UV-visible: A new quasi-analytical approach for the calculation of weighting functions, *J. Quant. Spectrosc. Radiat. Transfer*, *60*, 277–299, 1998.

Sander, R., and P. J. Crutzen, Model study indicating halogen activation and ozone destruction in polluted air masses transported to the sea, *J. Geophys. Res.*, *101*, 9121–9138, 1996.

Scheeren, H. A., J. Lelieveld, J. A. de Gouw, C. van der Veen, and H. Fischer, Methyl chloride and other chlorocarbons in polluted air during INDOEX, *J. Geophys. Res.*, *107*(D19), 8015, doi:10.1029/2001JD001121, 2002.

Schultz, M., M. Heitlinger, D. Mihelcic, and A. Volz-Thomas, A calibration source for peroxy radicals with built-in actinometry using H_2O and O_2 photolysis at 185 nm, *J. Geophys. Res.*, *100*, 18,811–18,816, 1995.

Shettle, E. P., and R. W. Fenn, Models of atmospheric aerosols and their optical properties, *AGARD Conf. Proc. 183, ADA028-615*, Advis. Group for Aerosp. Res. and Dev., Brussels, Belgium, 1976.

Singh, H. B., and L. J. Salas, Measurement of selected light hydrocarbons over the Pacific Ocean: Latitudinal and seasonal variations, *Geophys. Res. Lett.*, *9*, 842–845, 1982.

Singh, H. B., L. J. Salas, and R. E. Stiles, Methyl halides in and over the eastern Pacific (40°N ± 32°S), *J. Geophys. Res.*, *88*, 3684–3690, 1983.

Spicer, C. W., E. G. Chapman, B. J. Finlayson-Pitts, R. A. Plastridge, J. M. Hubbe, J. D. Fast, and C. M. Berkowitz, Unexpectedly high concentrations of molecular chlorine in coastal air, *Nature*, *394*, 353–356, 1998.

Stehr, J. W., W. P. Ball, R. R. Dickerson, B. G. Doddridge, C. A. Piety, and J. E. Johnson, Latitudinal gradients in O_3 and CO during INDOEX 1999, *J. Geophys. Res.*, *107*(D19), 8016, doi:10.1029/2001JD000446, 2002.

Vogt, R., P. J. Crutzen, and R. Sander, A mechanism for halogen release from sea salt aerosol in the remote marine boundary layer, *Nature*, *383*, 327–330, 1996.

Volz-Thomas, A., et al., PRICE III—Final report, Forschungsz. Jülich, Jülich, Germany, 1998.

Wagner, V., C. Schiller, and H. Fischer, Formaldehyde measurements in the marine boundary layer of the Indian Ocean during the 1999 INDOEX cruise of the R/V *Ronald H. Brown*, *J. Geophys. Res.*, *106*(D22), 28,529–28,538, 2001.

Wagner, V., R. von Glasow, H. Fischer, and P. J. Crutzen, Are CH_2O measurements in the marine boundary layer suitable for testing the current understanding of CH_4 photooxidation?: A model study, *J. Geophys. Res.*, *107*(D3), doi:10.1029/2001JD000722, 2002.

Weller, R., O. Schrems, A. Boddenberg, S. Gaeb, and M. Gautrois, Meridional distribution of hydroperoxides and formaldehyde in the boundary layer of the Atlantic (48°N–35°S) measured during the ALBATROSS campaign, *J. Geophys. Res.*, *105*, 14,401–14,412, 2000.

Welton, E. J., K. J. Voss, P. K. Quinn, P. Flatau, K. Markowicz, J. Campbell, J. D. Spinhirne, H. R. Gordon, and J. Johnson, Measurements of aerosol vertical profiles and optical properties during INDOEX 1999 using micropulse lidars, *J. Geophys. Res.*, *107*(D19), 8019, doi:10.1029/2000JD000038, 2002.

Wisthaler, A., A. Hansel, R. R. Dickerson, and P. J. Crutzen, Organic trace gas measurements by PTR-MS during INDOEX 1999, *J. Geophys. Res.*, *107*(D19), 8024, doi:10.1029/2001JD000576, 2002.

Yokouchi, Y., H.-J. Li, T. Machida, S. Aoki, and H. Akimoto, Isoprene in the marine boundary layer (Southeast Asian Sea, eastern Indian Ocean, Southern Ocean): Comparison with dimethyl sulfide and bromoform, *J. Geophys. Res.*, *104*(D7), 8067–8076, 1999.

Yokouchi, Y., Y. Noijiri, L. A. Barrie, D. Toom-Sauntry, T. Machida, Y. Inuzuka, H. Akimoto, H.-J. Li, Y. Fujinuma, and S. A. Aoki, A strong source of methyl chloride to the atmosphere from tropical coastal land, *Nature*, *403*, 295–298, 2000.

M. D. Andrés-Hernández, J. Burkert, J. P. Burrows, J. Meyer-Arnek, and L. Reichert, Institute of Environmental Physics (IUP), University of Bremen, Kufsteiner Str., P.O. Box 33 04 40, D-28334 Bremen, Germany. (lola@iup.physik.uni-bremen.de; burkert@iup.physik.uni-bremen.de; burrows@iup.physik.uni-bremen.de; julian@iup.physik.uni-bremen.de; reichert@iup.physik.uni-bremen.de)

T. Carsey, Atlantic Oceanographic and Meteorological Laboratories, National Oceanic and Atmospheric Administration, Miami, FL 33149, USA. (carsey@aoml.noaa.gov)

R. R. Dickerson and B. Doddridge, Department of Meteorology, University of Maryland, College Park, MD 20742, USA. (bruce@atmos.umd.edu; russ@atmos.umd.edu)

J. Mühle, Air Chemistry Division, Max Planck Institute for Chemistry, P.O. Box 2060, D-55020 Mainz, Germany. (muehle@mpch-mainz.mpg.de)

A. Zahn, Institute of Meteorology and Climate Research, Forschungszentrum Karlsruhe, University Karlsruhe, P.O. Box 3640, D-76021 Karlsruhe, Germany. (andreas.zahn@imk.fzk.de)

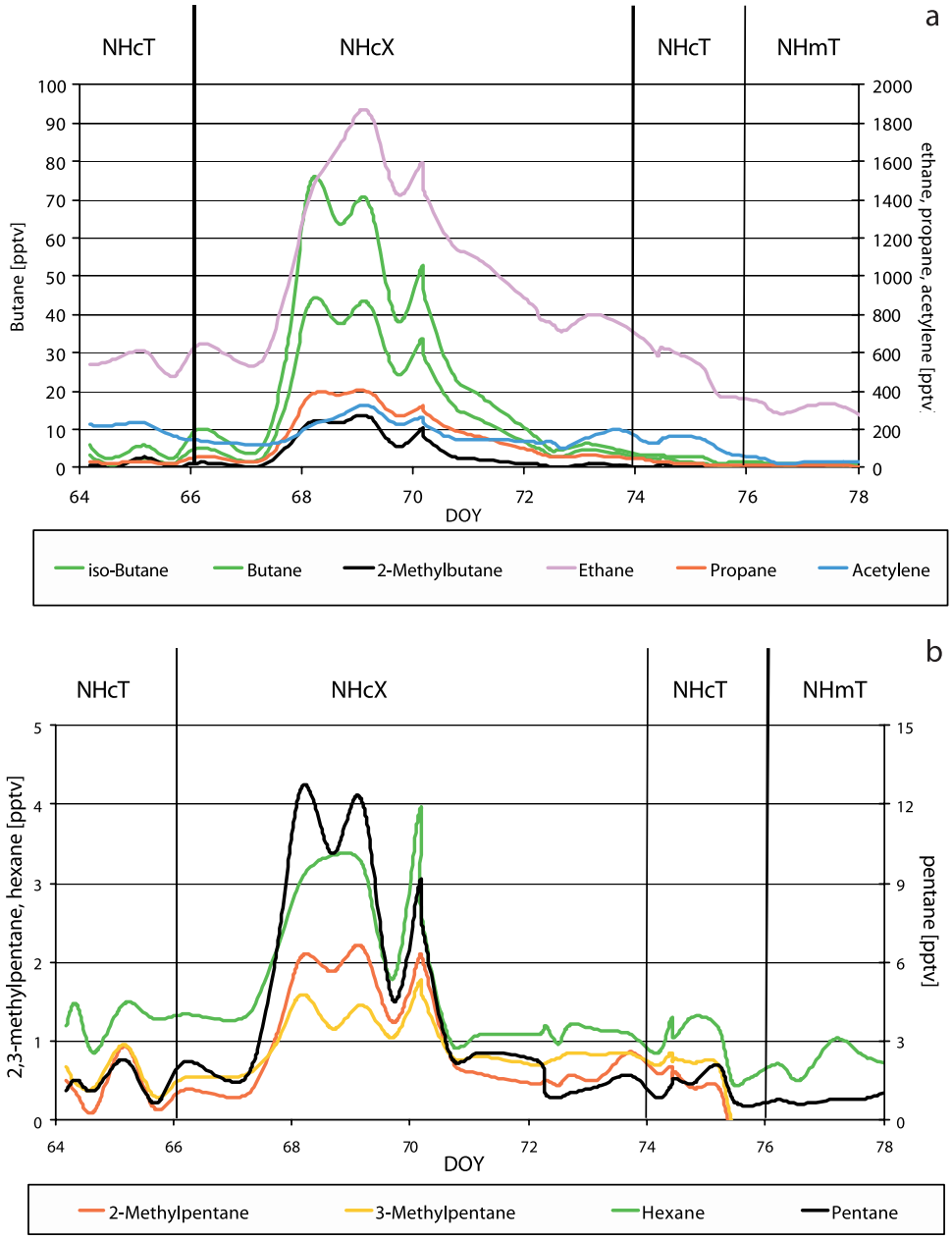

Figure 5. NMHC alkane measurements in the NH during INDOEX (DOY 64–78) (a) the lighter alkanes and (b) the heavier alkanes measured.

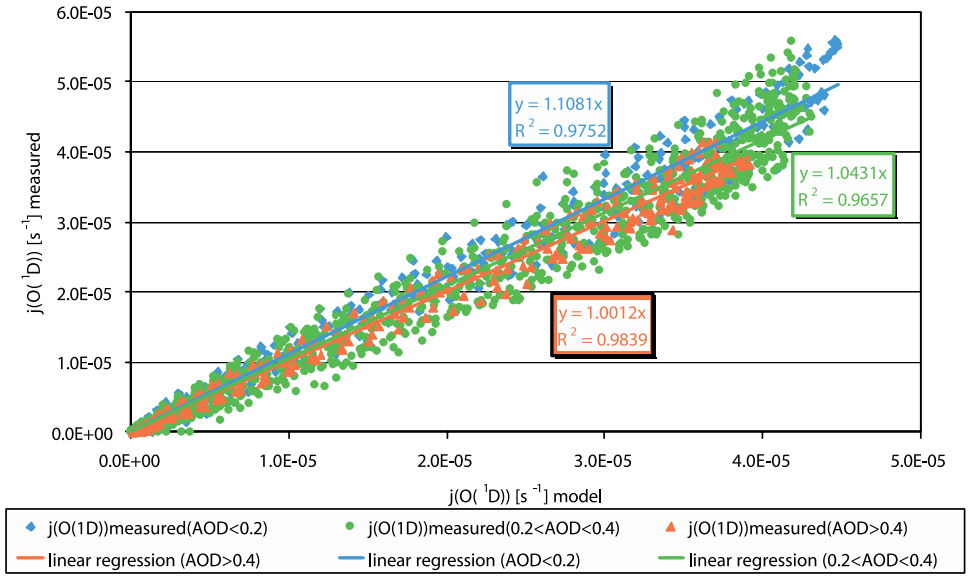

Figure 10. Correlation between measured and modeled j($O(^1D)$ photolysis rates during INDOEX, separated into different AOD ranges.

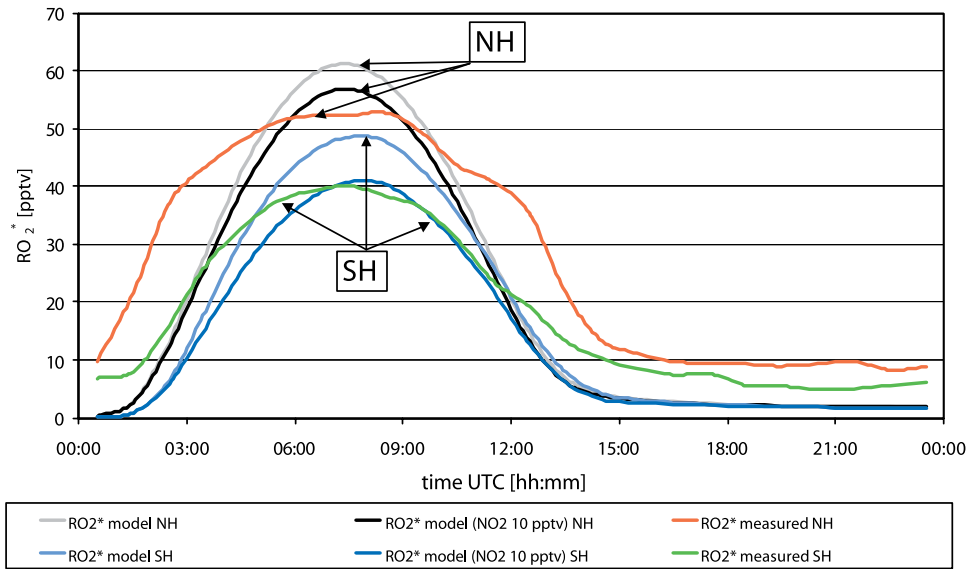

Figure 11. Average diurnal variation of measured and modeled RO_2^* mixing ratios for the NH and SH during INDOEX. Local time is given by UTC + ~4 hours.

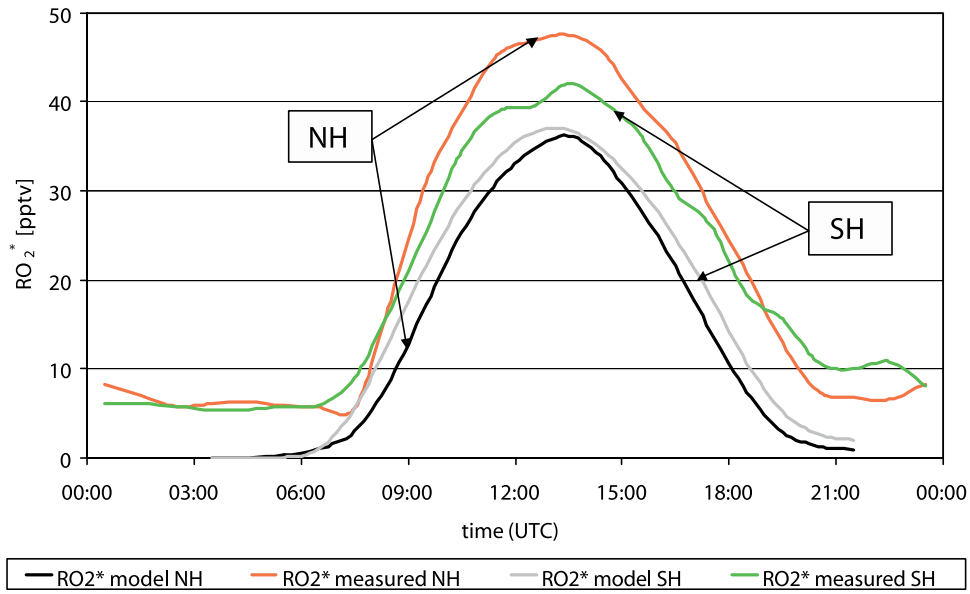

Figure 14. Average diurnal variation of measured and modeled RO_2^* mixing ratios for the NH and SH during ALBATROSS (1996) above the Atlantic Ocean. Local time is given by UTC + ~2 hours.